

学位論文

**The Elucidation of Reaction Mechanism of
Organic Photochemistry**

Using DMPO Spin Trapping Method

(DMPO スピントラップ法を用いた
有機光反応機構の解明)

学位取得年月 2023 年 3 月

広島大学大学院先進理工系科学研究科

先進理工系科学専攻

基礎化学プログラム

大山 諒子

Table of Contents

1. 主論文

The Elucidation of Reaction Mechanism of Organic Photochemistry
Using DMPO Spin Trapping Method

(DMPO スピントラップ法を用いた有機光反応機構の解明)

2. 公表論文

(1) “Reactivity and Product Analysis of a Pair of Cumyloxyl and *tert*-
Butoxyl Radicals Generated in Photolysis of *tert*-Butyl Cumyl
Peroxide”

Ryoko Oyama and Manabu Abe*

J. Org. Chem. **2020**, *85*, 8627-8638.

(2) “DMPO Spin Trapping Study of the Photolysis of 2-(4-Nitrophenyl)-
1*H*-indolyl-3-methyl Derivatives”

Ryoko Oyama, Ryuei Hayashi, and Manabu Abe*

Chem. Lett. **2023**, *52*, 10-12.

3. 参考論文

(1) “Design and Synthesis of Two-Photon Responsive Chromophores for Near-Infrared Light-Induced Uncaging Reactions”

Manabu Abe,* Youhei Chitose, Satish Jakkampudi, Pham Thi Thu Thuy, Qianghua Lin, Bui Thi Van, Ayato Yamada, Ryoko Oyama, Miyu Sasaki, and Claudine Katan*

Synthesis, **2017**, *49*, 3337–3346.

(2) “Simple generation of various α -monofluoroalkyl radicals by organic photoredox catalysis: modular synthesis of β -monofluoroketones”

Ryo Taniguchi, Naoki Noto, Seiya Tanaka, Keigo Takahashi, Sujan K. Sarkar, Ryoko Oyama, Manabu Abe, Takashi Koike,* and Munetaka Akita*

Chem. Commun. **2021**, *57*, 2609-2612.

主論文

**The Elucidation of Reaction Mechanism of
Organic Photochemistry
Using DMPO Spin Trapping Method**

March, 2023

Department of Chemistry,
Graduate School of Advanced Science and
Engineering,
Hiroshima University

Ryoko OYAMA

Contents

Chapter 1. General Introduction

1-1. Organic Photochemistry	13
1-2. Detection of Radical Species	14
1-3. Spin Trapping	15
1-4. Identification of DMPO Spin Adducts	17
1-5. Purpose of this research	19

Chapter 2. DMPO Spin Trapping Study in the Photolysis of *tert*-Butyl Cumyl Peroxide

2-1. Introduction	23
2-2. Synthesis and Absorption spectrum of 1	24
2-3. Detection of Alkoxy Radicals by Spin Trapping	25
2-4. Detection of CumO• by LFP measurements	30
2-5. Product Analysis in the Photolysis of 1	30
2-6. Mechanism	32
2-7. Conclusion	33
2-8. Experimental Section	33
2-9. Supplementary Material	38

Chapter 3. DMPO Spin Trapping Study in the Photolysis of 2-(4-Nitrophenyl)-1*H*-indolyl-3-methyl Derivatives

3-1. Introduction	47
3-2. Synthesis and Absorption spectrum of 18a	49

3-3. Detection of Radical Species by Spin Trapping·····	50
3-4. Mechanism·····	55
3-5. Conclusion·····	56
3-6. Experimental Section·····	57
3-7. Supplementary Material·····	61

Chapter 4. Conclusions and Outlook

References

List of Publications

Acknowledgment

Chapter 1
General Introduction

1-1. Organic Photochemistry

Natural systems are supported by “light energy” such as sunlight, as exemplified by photosynthesis. Substances around us absorb light energy and reach an electronically excited state with high energy that can express various functions. Since the electronically excited state has higher energy and a different electron configuration compared to the ground state, organic photochemical reactions can induce the formation of compounds that are not formed in thermal reactions through the unique reactions in the electronically excited state (Figure 1).¹

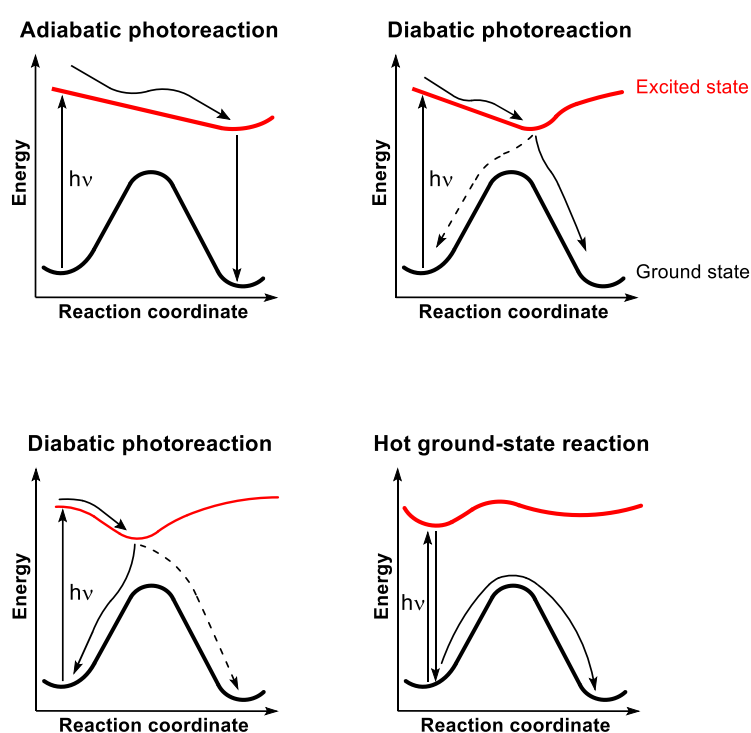
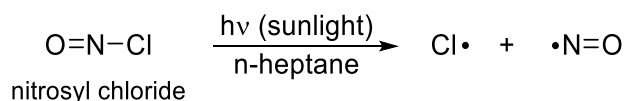


Figure 1. Difference types of photoreactions.

Elucidating the mechanism by which photochemical reactions occur will help us to understand the providence of nature and lead to creating a new science that enables us to coexist in harmony with nature. If we can clarify the reactivity of electronically excited states and reactive intermediates, which have short-lived and less understood reactivity, produced by photoirradiation of substances, it will be possible to create new chemistry that contributes to the development of a sustainable society.

Several organic photochemical reactions have been reported to generate reactive radical species. Historically, the first report was the photonitrosation of nitrosyl chloride (O=N-Cl) discovered by Lynn in 1919.²



However, many radical species are kinetically unstable and short-lived, which makes it difficult to observe experimentally them under the reaction conditions. Therefore, most of the reaction mechanisms reported so far have been proposed inductively from product analysis results after photoreaction or from theoretical calculations.

In this study, experimental detection and identification of radical species have been attempted to elucidate in detail the reaction mechanism of photoreaction that generate radical species. Understanding the reaction mechanism will not only improve chemical yields and selectivity, but also lead to the development of new reactions that will open the way to the future.

1-2. Detection of Radical Species

The detection and structural analysis of radical species are usually performed by electron paramagnetic resonance (EPR) spectroscopy,³ a phenomenon in which unpaired electrons absorb the energy of electromagnetic waves in a magnetic field and resonate with them.

Electrons in a magnetic field split into two energy levels $E_1 = +1/2g\mu_B H$ and $E_2 = -1/2 g\mu_B H$ (Zeeman splitting). The electrons are distributed into the two energy levels due to the Maxwell-Boltzmann distribution and are in thermal equilibrium. When an electron in such a state is irradiated with an electromagnetic wave of a specific wavelength with an energy that satisfies the equation $\Delta E = g\mu_B H_0 = h\nu$, the electron in energy level E_2 absorbs the energy of the electromagnetic wave and transitions to energy E_1 by absorbing the energy of the electromagnetic wave (Figure 2). This phenomenon is called electron paramagnetic resonance absorption.

The electron spins of the radical species interact with the nuclear spins of the surrounding elements, resulting in a splitting pattern in the absorption spectrum (hyperfine structure) based on this interaction. This can be analyzed to derive structural information. However, in the case of short-lived radicals such as a phenyl radical, it is difficult to observe them by the conventional EPR method. In this case, the “Spin Trapping” method allows the detection of such short-lived radical species.

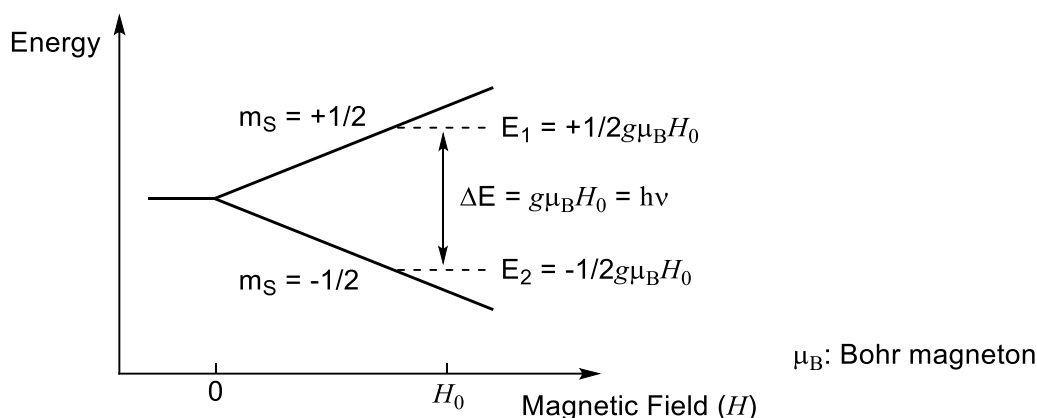
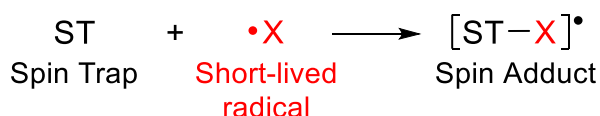


Figure 2. Zeeman Splitting of the electron levels of an unpaired electron in a magnetic field.

1-3. Spin Trapping

In the spin trapping method, when the spin trap agent ST traps the radical species $\bullet X$, it gives a relatively stable and long-lived spin adduct $[ST-X]\bullet$, which can be observed by the EPR method. When observing EPR spectra with this method, different values of hyperfine coupling constants are obtained depending on the spin trap agent used and the trapped radical species. These values are important clues to the chemical structure of the radical species and spin adducts.



In the molecules of spin trap agents, there exist ^1H ($I = 1/2$) and ^{14}N ($I = 1$) with nuclear spins. The produced spin adduct interacts with the magnetic moment (μ_S) of the unpaired electron and the magnetic moment (μ_I) of the nucleus in the vicinity of the unpaired electron. As a result, when ^{14}N is present near the unpaired electron, the N nuclear spin is split into three levels $-1, 0, +1$ (for $I = 1, 2I + 1 = 3$), so that each level of the electron spins is also split into three more levels, yielding three hyperfine lines with equal intensity (Figure 3). The magnitude of these hyperfine structures is the hyperfine coupling constant (HFCC), which is generally expressed as a value and depends on the magnitude of the hyperfine interaction. The effects of the nuclear spin of the trap agent on the magnetic moment of the unpaired electron in the spin adduct usually appear when the nuclear spin is in the third atom counting from the atom with the unpaired electron. The further away from the unpaired electron the nucleus with nuclear spin is,

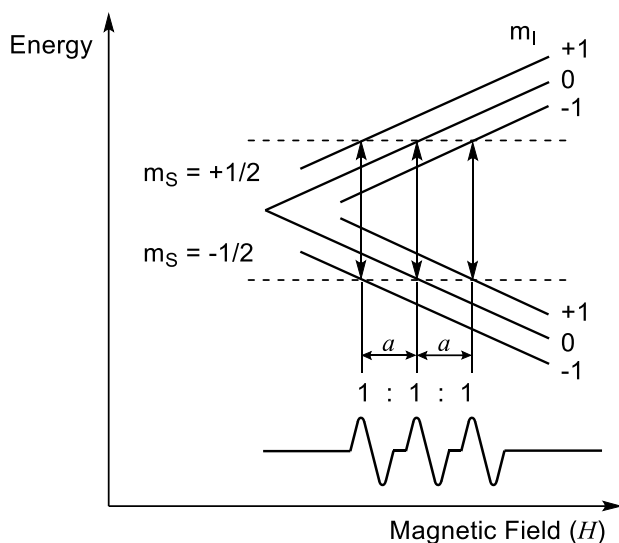


Figure 3. Hyperfine structure with ^{14}N nuclei ($I = 1$).

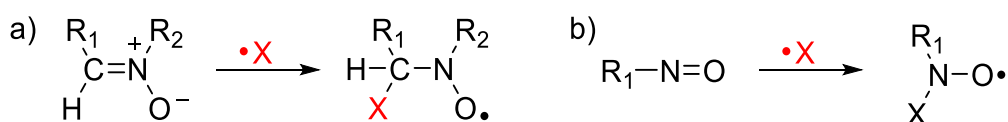


Figure 4. Formation of nitroxides from the reaction of a) nitrene and b) nitroso compounds with free radicals.

the smaller the effect becomes.

The spin trapping method was developed by Janzen *et al.* in Canada in the late 1960s,⁴ inspired by the work of Japanese researchers Iwamura and Inamoto, who reported that nitrene compounds react with radical species $\cdot\text{X}$ to form stable nitroxide radicals (Figure 4).^{5,6} This allows radical species that could not be measured by conventional EPR spectrometry because of their instability to be covalently bonded to nitrene or nitroso compounds and measured as stable nitroxide radicals at room temperature.

Among these spin trap agents, the most frequently used is 5,5-dimethylpyrroline-N-oxide (DMPO), one of the nitrene compounds (Figure 5). The reason for this is that DMPO reacts with many radical species $\cdot\text{X}$ with different chemical structures and the spin adduct exhibits significantly different EPR spectra of hyperfine structures. The greatest advantage of the spin trapping method using DMPO is that it is possible to discriminate and identify multiple radicals existing in the same reaction solution by

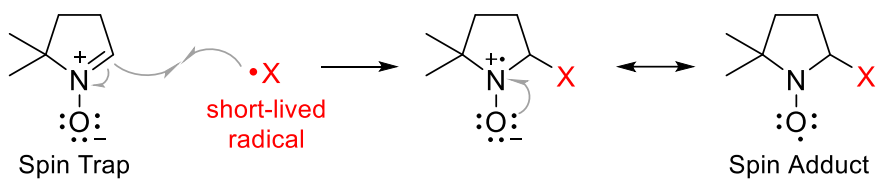


Figure 5. Radical addition to DMPO for the formation of the spin adduct.

analyzing the hyperfine coupling constants of the EPR spectra of DMPO spin adducts. In addition to these advantages, the spin trapping method with DMPO has become widespread in the medical and biological fields as a detection method for free radicals generated in reactions in biological systems because of the high water-solubility of DMPO.

Therefore, in this study, we employed the spin trapping method using DMPO to experimentally prove that radical species are generated as intermediates under actual photoreaction conditions, and to identify the radical species generated.

1-4. Identification of DMPO Spin Adducts

The HFCC values of various DMPO spin adducts have been reported,⁷ but in most cases, spin adducts with HFCC values that have not been reported are formed in photoreaction of organic compounds. In addition, when there are multiple spin adducts with unknown HFCC values, it is difficult to identify the radicals by EPR measurements alone. To solve this problem, the spin adducts produced by photoreactions are not only analyzed by EPR method, but also by mass spectrometry (MS) method; an example using MS method was reported by Guo *et al.* in 2003, successfully identified the DMPO spin adduct of the oxygen-centered radicals.⁸

Furthermore, the HFCC values (a_N and a_H^{β} values) of the DMPO spin adducts, whose structures are proposed by the MS analysis, are computed using quantum chemical calculations. The computed HFCC can be compared them with the values obtained from the experimentally obtained EPR measurements to determine the structure of the produced spin adducts. The computational method reported by Yamaguchi in 2017 was used for the HFCC values of the DMPO spin adduct.⁹

All the spin adduct calculations were performed by using the Gaussian 16 program.¹⁰ Long-range corrected hybrid functional (LC- ω PBE)¹¹ and Pople's double-zeta and polarization function (6-31G(d))¹² with solvent model density (SMD)¹³ for solvent effect were used throughout the study. The HFCC values of the DMPO spin adducts were calculated by following steps 1-4 below.

1. Geometries of 4T_3 and 3T_4 ring conformers (Figure 6) and rotational conformers of DMPO spin adducts are optimized.

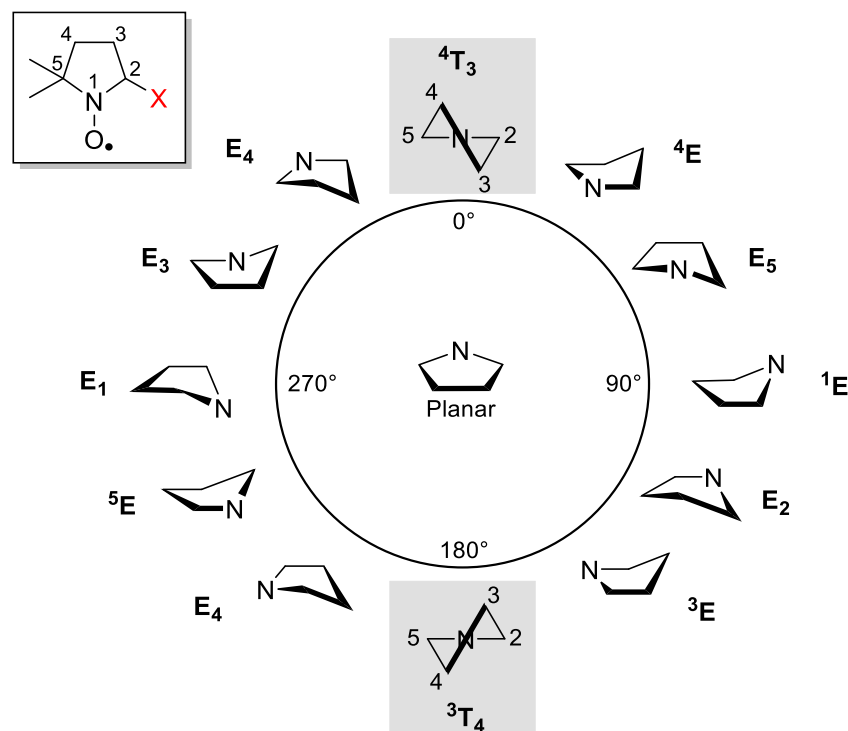


Figure 6. Five-membered ring conformation of DMPO spin adduct [envelope (E) or twist (T)].¹⁴ We denoted by xT_y (or xE_y) a conformation in which the ring carbon or nitrogen x position is above, and y position is below the ring mean plane.

2. For each DMPO spin adduct conformation, a 298.15 K Boltzmann contribution was determined. The weighting of each conformer was determined via a Boltzmann average. Here, several conformers, whose relative population was estimated to be less than 0.01 upon a Boltzmann average, were excluded.
3. For each optimized DMPO spin adduct conformer with a Boltzmann average larger than 0.01, a single-point energy calculation is performed in the Gaussian program with the *Output=Pickett*¹⁵ keyword to output the HFCC.
4. Finally, the averaged HFCC values are calculated.

(e.g.) if there are three conformers **A**, **B**, and **C**,

$$\begin{aligned} \text{The averaged HFCC} = & \{(\text{HFCC value}_A) \times (\text{relative population}_A)\} + \\ & \{(\text{HFCC value}_B) \times (\text{relative population}_B)\} + \\ & \{(\text{HFCC value}_C) \times (\text{relative population}_C)\} \end{aligned}$$

1-5. Purpose of this research

In this study, the DMPO spin trapping experiments were conducted in two organic photoreactions shown in Chapters 2 and 3, in which radical species are thought to be generated as reaction intermediates to understand the mechanism of photochemical reactions. In addition to the spin trapping experiments, the quantitative product analysis of the organic photoreactions was performed to support and confirm the proposed reaction mechanism by the spin-trapping experiments in the photolysis.

Chapter 2

DMPO Spin Trapping Study in the Photolysis of *tert*-Butyl Cumyl Peroxide

2-1. Introduction

Humans and other organisms that use atmospheric oxygen to produce energy produce high reactivity reactive oxygen species (ROS) as a byproduct in their bodies, which play an essential role in the body's immune function and infection defense.¹⁶ However, when the body produces excessive amounts of ROS due to ultraviolet light, smoking, stress, etc., the balance between oxidation and antioxidant effects in the body is disrupted, causing oxidative stress. Oxidative stress converts normal cells into cancer cells.

So far, cancer prevention and treatment methods have been used to reduce oxidative stress by decreasing ROS levels in cancer cells through the supplemental administration of antioxidants.¹⁷ However, it has recently been reported that antioxidant supplementation promotes the expansion of cancer cells. In fact, cancer cells have been found to maintain high ROS levels and continue to proliferate after supplemental administration of antioxidants.¹⁸ Therefore, as a new cancer treatment method, it has been considered efficient to inhibit the antioxidant effect produced in cancer cells and to excessively increase only the ROS level in cancer cells.

We assumed that if ROS could be generated locally in cancer cells using light, it would be possible to kill cancer cells without damaging normal cells. Hence, we focused on the photoreaction of *tert*-butyl cumyl peroxide (**1**), which can generate two

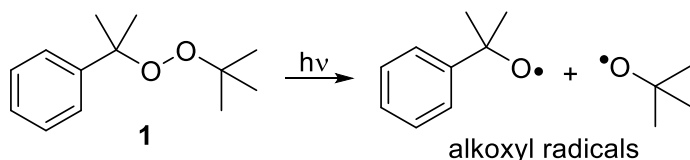


Figure 7. Photolysis of *tert*-butyl cumyl peroxide (**1**).

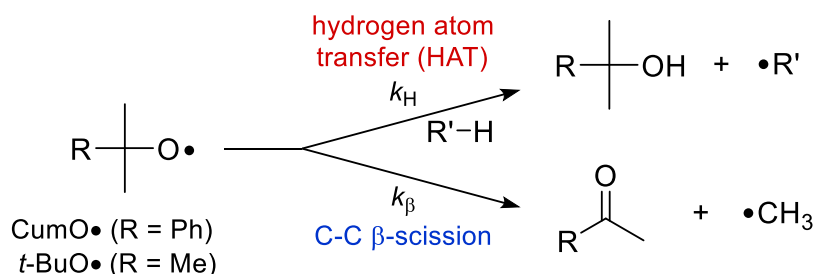


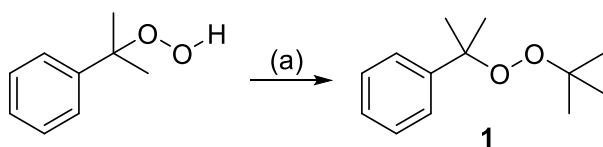
Figure 8. Reactivity of cumyloxy and *tert*-butoxy radicals in hydrogen atom transfer (HAT) and C-C β -scission.

alkoxyl radicals, the cumyloxyl radical (CumO•, R = Ph) and the *tert*-butoxyl radical (*t*-BuO•, R = Me), corresponding to ROS upon photoirradiation (Figure 7).¹⁹

Alkoxyl radicals are known to undergo either hydrogen atom transfer or carbon-carbon β -scission after formation (Figure 8).^{20, 21} However, the structure and yields of all products derived from alkoxyl radicals are not known. To control ROS levels in cancer cells, information about the yields of these two alkoxyl radicals is essential. In this study, we observed the two alkoxyl radicals generated by the photoirradiation of **1** using the DMPO spin trapping method and clarified the structure and yields of the products derived from the two alkoxyl radicals by nuclear magnetic resonance (NMR).

2-2. Synthesis and Absorption spectrum of **1**

Tert-butyl cumyl peroxide (**1**) was synthesized as shown in Scheme 1.²² UV-visible absorption spectroscopy was performed on the synthesized compound **1** (Figure 9). Structured absorption bands were observed in acetonitrile at about 240-270 nm.



Scheme 1. Synthesis of **1**; Reagents and conditions: (a) *tert*-Butyl 2,2,2-trichloroacetimidate, boron trifluoride-ethyl ether complex, -20°C to RT, a few minutes, 19% yield.

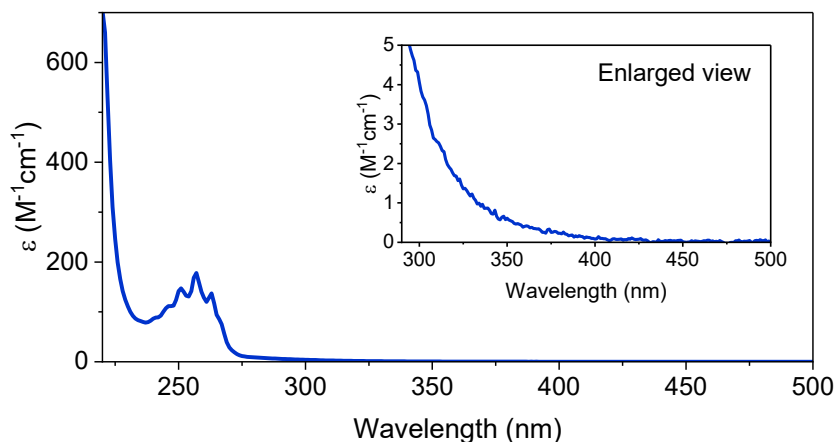


Figure 9. UV-vis absorption spectrum of **1** in acetonitrile.

2-3. Detection of Alkoxy Radicals by Spin Trapping

First, the photoreaction of **1** (12 mM) in the presence of ~10 equiv of DMPO (141 mM) was conducted in an EPR resonant cavity using a high-pressure Hg lamp in acetonitrile at 298 K under air atmosphere. After photoirradiation of the solution in a flat quartz cell, typical EPR signals of nitroxides ($R_2N-O\cdot$) were detected (Figure 10a). To analyze how many DMPO spin adducts are included in the spectra observed in this photoreaction and their HFCC values, the spectra were compared to those observed in the photolysis of di-*tert*-butyl peroxide and dicumyl peroxide in the presence of DMPO

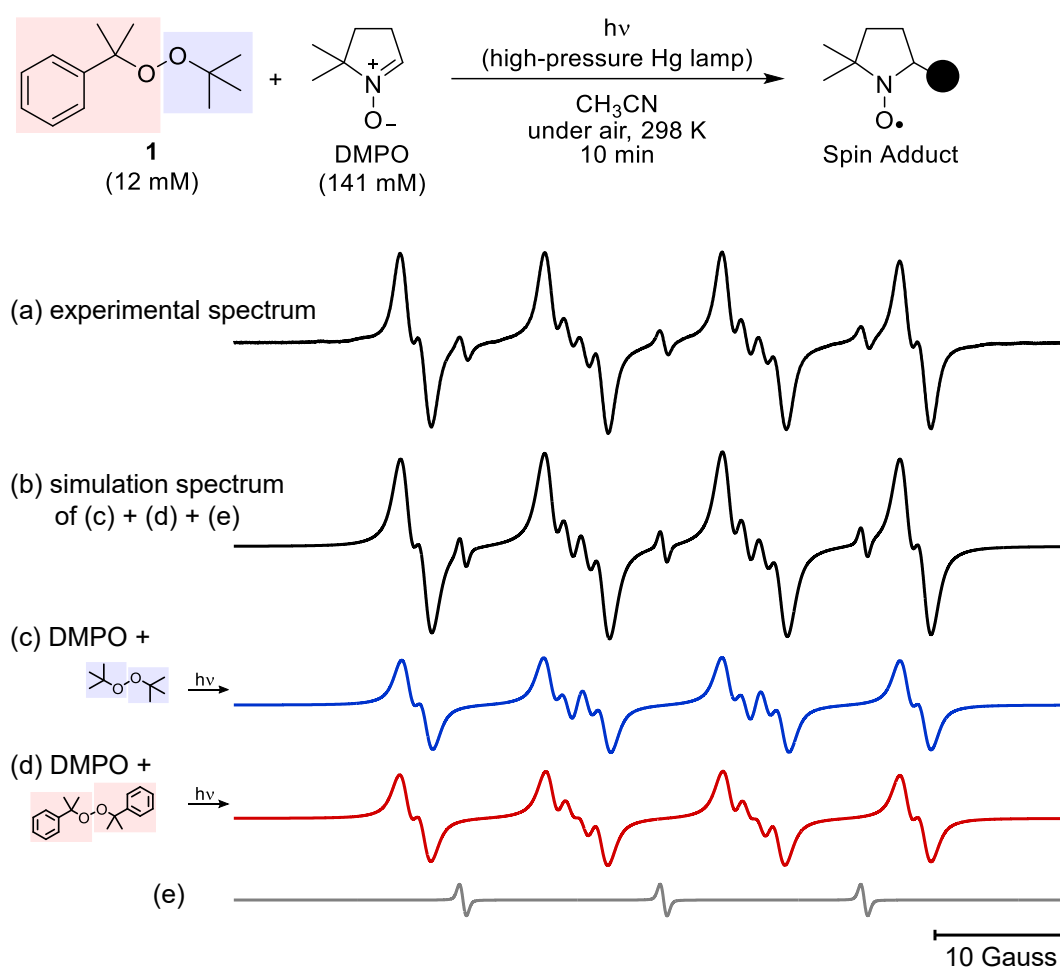


Figure 10. (a) EPR spectra obtained after the photolysis of **1** (12 mM) and DMPO (141 mM) in acetonitrile. (b) Simulation spectrum of sum of (c; $a_N = 13.50$ G, $a_{H^\beta} = 10.75$ G, $a_{H^\gamma} = 1.27$ G), (d; $a_N = 13.42$ G, $a_{H^\beta} = 11.05$ G, $a_{H^\gamma} = 1.28$ G), and (e; $a_N = 15.20$ G) with at 8.7: 8.7: 1 ratio. (c) EPR spectrum obtained after the photolysis di-*tert*-butyl peroxide (16 mM) and DMPO (113 mM). (d) EPR spectrum obtained after the photolysis dicumyl peroxide (11 mM) and DMPO (108 mM). (e) Simulation spectrum.

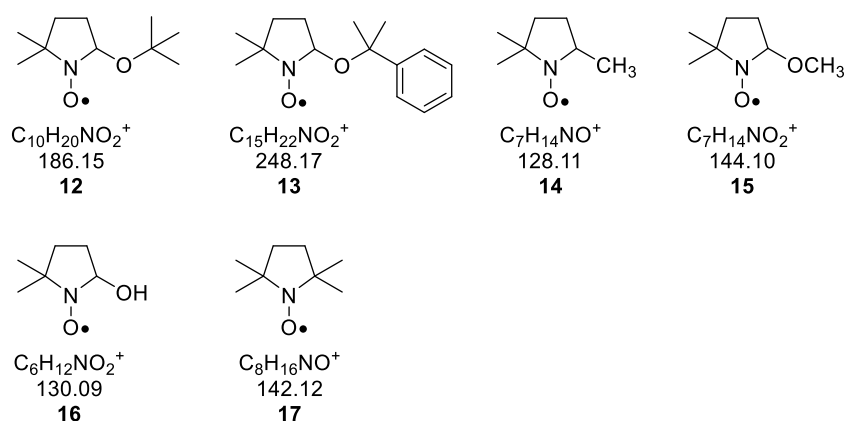


Figure 11. Spin adducts **12-17** were detected by electrospray ionization-MS (FTMS, positive mode) measurements.

(Figures 10c,d). The spectra observed upon photoirradiation of the two symmetric peroxides are predicted to derive from the spin adducts in which CumO• and *t*-BuO• are trapped (**12** and **13**, respectively) or methyl radical released from the C-C β-scission of each alkoxy radicals are trapped (**14**). As a result of the analysis using WinEPR simulation software,²³ the EPR signal obtained from the photolysis of **1** in the presence of DMPO contained EPR spectra obtained from the photolysis of two peroxides and a spectrum containing triplet signals with a hyperfine constant of 15.2 G (Figure 10e).

To obtain information about the structures detected in the photolysis **1** in the presence of DMPO, an MS analysis was conducted on the photolysate (Figure 11). In addition to the mass numbers of the two alkoxy radical trapped nitroxides **12** (MS 186.15) and **13** (MS 248.17), and methyl radical trapped nitroxide **14** (MS 128.11), three radical trapping compounds **15-17** were detected, indicating that there is a possibility to form methoxy and hydroxyl radicals during the photolysis of **1**. These results indicate that the spectrum in Figure 10(e) observed in the EPR measurement corresponds to spin adduct **17**,²⁴ in which the hydrogen atom at β-position is replaced by a methyl group. On the other hand, for the spectra of Figures 10(c) and 10(d), it is not yet identified whether each spectrum is derived from a spin adduct in which an alkoxy radical (CumO• or *t*-BuO•) is trapped or a methyl radical is trapped.

To reveal the molecular structures of the DMPO spin adducts showing the spectra in Figures 10(c) and 10(d), the HFCC values of spin adducts **12**, **13**, and **14** were calculated by quantum chemical calculations and compared with experimental values. DMPO spin adducts **12-14** were optimized to obtain the equilibrium ring and rotational conformers at LC-ωPBE with the 6-31G(d) basis set in acetonitrile (SMD), whose

HFCC values were calculated at the same level of theory using the Gaussian 16 program.

According to the calculation results using the procedure described in chapter 1, spin adducts DMPO-*Ot*Bu (**12**), DMPO-OCum (**13**), and DMPO-CH₃ (**14**) have three, six, and two energetically stable conformations, respectively (Figures 11-13, Tables 1-3). The average HFCC, a_N and a_{H^β} values for each spin adduct were calculated by Eqs. 1 and 2 for spin adduct DMPO- *Ot*Bu (**12**), by Eqs. 3 and 4 for spin adduct DMPO-OCum (**13**), and by Eqs. 5 and 6 for spin adduct DMPO-CH₃ (**14**).

The computed average HFCC values of the DMPO spin adducts are summarized in Table 4. The calculated HFCC values of spin adducts **12-14** were compared with the experimentally obtained HFCC values. From the correlation between experimental and calculated HFCC values (Figures 14a,b), the spectrum in Figure 10(c) and Figure 10(d) correspond to the spin adduct **12** and **13**, respectively. Since a methyl radical is highly reactive, the concentration of spin adduct DMPO-CH₃ (**14**) is too low to be detected by EPR measurements in the photolysis of **1** in the presence of DMPO. These results indicated that two alkoxy radicals, CumO• and *t*-BuO•, are generated in the photoreaction of **1**, and that a methyl radical is generated through the C-C β- scission of each alkoxy radical.

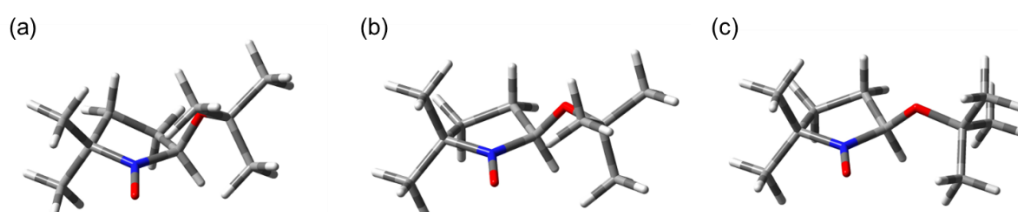


Figure 11. Three optimized conformers of spin adduct DMPO-*Ot*Bu (**12**).

Table 1. Three conformers of spin adduct DMPO-*Ot*Bu (**12**).

Conformation	Total energy (Hartree)	Relative population	a_N (Gauss)	a_{H^β} (Gauss)
(a) 4T_3	-597.909384	0.777	10.11	4.59
(b) 3T_4	-597.906743	0.047	10.23	14.43
(c) 3T_4	-597.907981	0.176	10.00	18.12

$$a_N = (10.11 \text{ G} \times 0.777) + (10.23 \text{ G} \times 0.047) + (10.00 \text{ G} \times 0.176) \approx 10.10 \text{ G} \quad (1)$$

$$a_{H^\beta} = (4.59 \text{ G} \times 0.777) + (14.43 \text{ G} \times 0.047) + (18.12 \text{ G} \times 0.176) \approx 7.43 \text{ G} \quad (2)$$

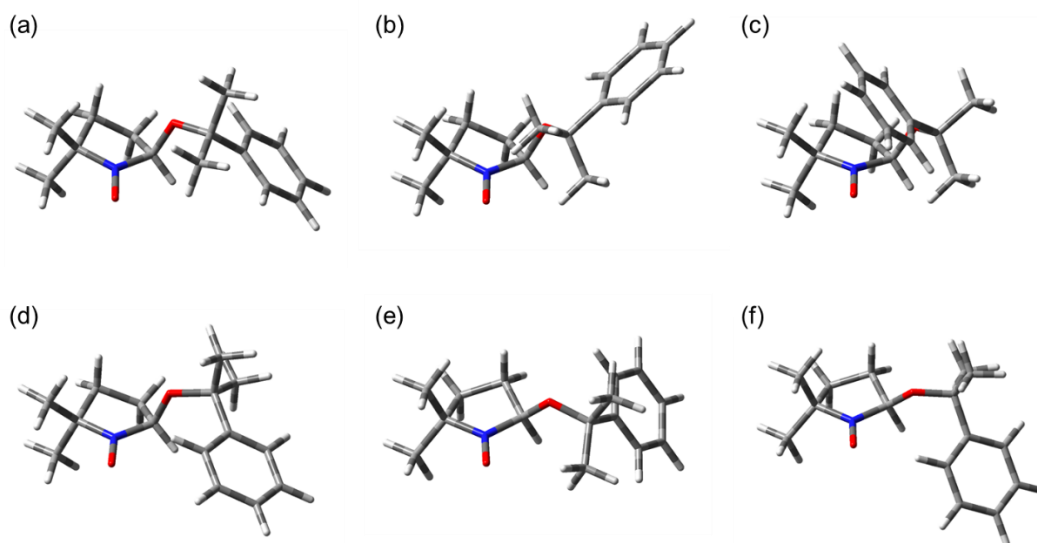


Figure 12. Six optimized conformers of spin adduct DMPO-OCum (**13**).

Table 2. Six conformers of spin adduct DMPO-OCum (**13**).

	Conformation	Total energy (Hartree)	Relative population	a_N (Gauss)	a_{H^β} (Gauss)
(a)	4T_3	-789.498068	0.316	9.88	4.52
(b)	4T_3	-789.497597	0.192	10.02	4.71
(c)	4T_3	-789.496752	0.078	10.38	5.99
(d)	4T_3	-789.497372	0.151	9.56	7.65
(e)	3T_4	-789.497319	0.143	9.96	17.82
(f)	3T_4	-789.497158	0.120	10.08	18.62

$$a_N = (9.88 \text{ G} \times 0.316) + (10.02 \text{ G} \times 0.192) + (10.38 \text{ G} \times 0.078) + (9.56 \text{ G} \times 0.151) + (9.96 \text{ G} \times 0.143) + (10.08 \text{ G} \times 0.120) \approx 9.94 \text{ G} \quad (3)$$

$$a_{H^\beta} = (4.52 \text{ G} \times 0.316) + (4.71 \text{ G} \times 0.192) + (5.99 \text{ G} \times 0.078) + (7.65 \text{ G} \times 0.151) + (17.82 \text{ G} \times 0.143) + (18.62 \text{ G} \times 0.120) \approx 8.74 \text{ G} \quad (4)$$

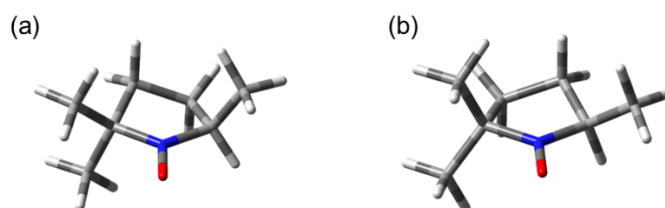


Figure 13. Two optimized conformers of spin adduct DMPO-CH₃ (**14**).

Table 3. Two conformers of spin adduct DMPO-CH₃ (**14**).

	Conformation	Total energy (Hartree)	Relative population	a_N (Gauss)	a_{H^β} (Gauss)
(a)	⁴ T ₃	-404.865327	0.268	10.58	13.80
(b)	³ T ₄	-404.866277	0.732	10.62	23.47

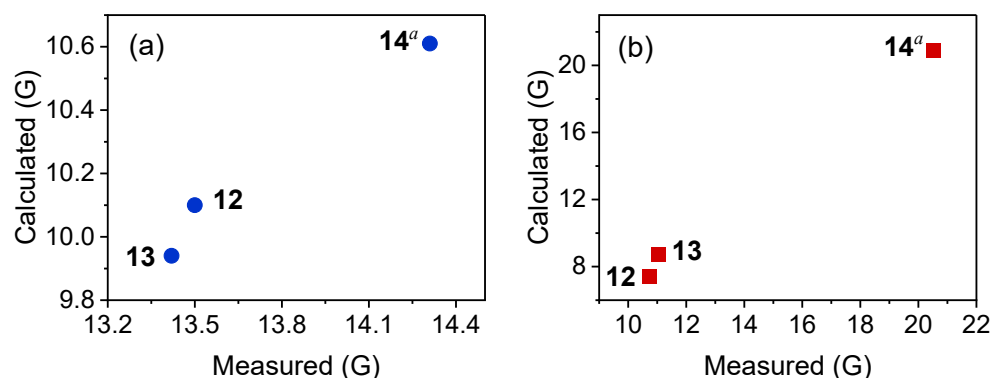
$$a_N = (10.58 \text{ G} \times 0.268) + (10.62 \text{ G} \times 0.732) \approx 10.10 \text{ G} \quad (5)$$

$$a_{H^\beta} = (13.80 \text{ G} \times 0.268) + (23.47 \text{ G} \times 0.732) \approx 7.43 \text{ G} \quad (6)$$

Table 4. Calculated HFCC values of the DMPO spin adducts based on ULC- ω PBE/6-31G(d) (SMD: acetonitrile) and HFCC values analyzed from EPR measurements in the photolysis of **1** (12 mM) and DMPO (141 mM) in acetonitrile.

		12	13	14
Exp.	a_N	13.50	13.42	(14.31 ^a)
	a_{H^β}	10.75	11.05	(20.52 ^a)
Calc.	a_N	10.10	9.94	10.61
	a_{H^β}	7.43	8.74	20.88

^aThe HFCC values of spin adduct **14** in parentheses are the reported values in benzene.^{7a}

**Figure 14.** HFCC values of (a) nitrogen (a_N) and (b) β -hydrogen (a_{H^β}) in DMPO spin adducts in acetonitrile. ^aThe experimental HFCC values of spin adduct **14** are the reported values in benzene.^{7a}

2-4. Detection of CumO• by LFP measurements

The detection of cumyloxyl radical CumO• was also conducted by laser flash photolysis (LFP) measurements. In the LFP measurements, 266 nm of light (Nd-YAG, 10 mJ/ pulse, 10 ns pulse width) was irradiated into the solution **1** (8.5 mM, acetonitrile, Abs = 1.1 at 266 nm) under air conditions at ~293 K. After laser irradiation, the generation and fall of CumO• were detected at 485 nm ($k_{\text{fall}} = 6.7 \times 10^5 \text{ s}^{-1}$, Figure 15), which is consistent with the reported value of CumO•.¹⁹

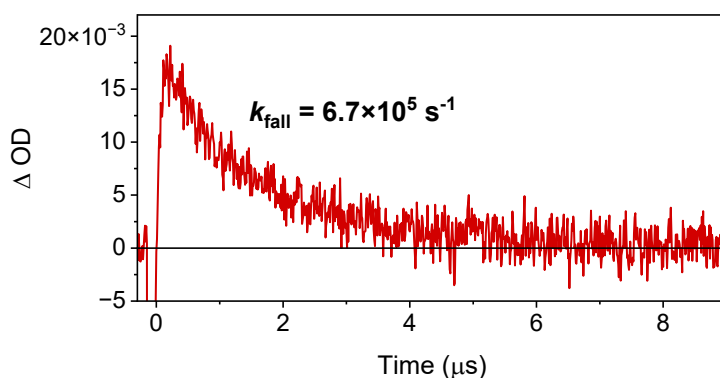


Figure 15. Fall process of CumO• observed at 485 nm in the laser flash photolysis of **1**.

2-5. Product Analysis in the Photolysis of **1**

The photoreaction of **1** (20.5 mM) was conducted using a 266 nm laser (1 mJ/ pulse, 10 Hz) in CD₃CN (0.5 mL) at ~298 K under air or O₂ atmospheric conditions (Table 5).

After 1 h of photolysis in the NMR tube, eleven photoproducts **2-11,11-d** were detected and identified by ¹H NMR analysis (Table 5). The photoproducts were derived from the A (CumO• side), B (*t*-BuO side), and A/B sides. The A-side products consisted of acetophenone (**2**), α -cumyl alcohol (**3**), and methyl cumyl ether (**4**). The B-side products consisted of acetone (**5**), *tert*-butanol (**6**), and *tert*-butyl methyl ether (**7**). Methanol (**8**), formaldehyde (**9**), ethane (**10**), methane (**11**), and mono-deuterated methane; CH₃D (**11-d**) were found to be formed from the •CH₃ generated from the C-C β -scission of the two alkoxy radicals, CumO• and *t*-BuO•. The chemical yields of the photoproducts and the conversion of **1** were determined using triphenylmethane as an internal standard. The conversions of **1** under air and O₂ atmospheric conditions, were 70.8 and 72.2%, respectively (entries 1 and 2). Under air atmospheric conditions ([O₂] = 1.9 mM, entry 1), acetophenone (**2**) was solely formed in 94.1 % of the A-side products,

Table 5. Products and Chemical Yields in Photolysis of **1** at 266 nm Irradiation^a

Reaction scheme showing the photolysis of compound **1** (20.5 mM) under air or O₂ conditions. The reaction is initiated by UV light (266 nm, 1 mJ) in CD₃CN (99.9%D) at ~298 K for 1 h. The products are analyzed by ¹H NMR. The products are categorized into A-side (2, 3, 4) and B-side (5, 6, 7). A/B-side products (8, 9, 10, 11, 11-d) are derived from a methyl radical.

entry	conv/%	A-side			B-side			A/B-side					
		2	3	4	5	6	7	8	9	10	11	11-d	
1	air	70.8	94.1	5.1	2.5	57.7	18.7	17.7	4.8	0.5	37.2	3.1	1.6
2	O ₂	72.2	96.6	7.3	1.9	60.6	30.0	14.3	14.6	1.7	31.3	4.3	0.8

^aChemical yields of the photoproducts were calculated using triphenylmethane as an internal standard.

Experimental error (%) is photoproduct chemical yield (%) × (± 5-8%).

together with a small amount of alcohol **3** and ether **4**. The selective formation of acetone (**5**) was found in 57.7% of the B-side products, together with a significant amount of the corresponding alcohol **6** (18.7%) and ether **7** (17.7%). The products **8-11** and **11-d** derived from $\cdot\text{CH}_3$ were identified by comparing the NMR signals of the genuine samples (Figures 26a-d). The oxygenated compounds **8** and **9** were derived from the reaction of the methyl radical with molecular oxygen.

Under O₂ atmospheric conditions ([O₂] = 9.1 mM, entry 2), an increase in the chemical yields of alcohols **3** and **6** and oxygenated compounds **8** and **9** were observed with the decrease in the formation of ethane (**10**) and ethers **4** and **7**, indicating that $\cdot\text{CH}_3$ generated from C-C β -scission from the alkoxy radicals escaped to the out-of-cage space to be trapped by O₂ to yield oxygenated compounds **8** and **9**. The decrease in the formation of ethers **4** and **7** also supports this mechanism. The reaction of $\cdot\text{CH}_3$ with O₂ was computed at UB3LYP²⁵/6-31G(d)¹² to be exothermic in the formation of methyl peroxide, $\Delta H_{298} = -31.25 \text{ kcal mol}^{-1}$, without an energy barrier (Figure 16). The peroxide is the precursor for methanol (**8**) and formaldehyde (**9**).^{26, 27}

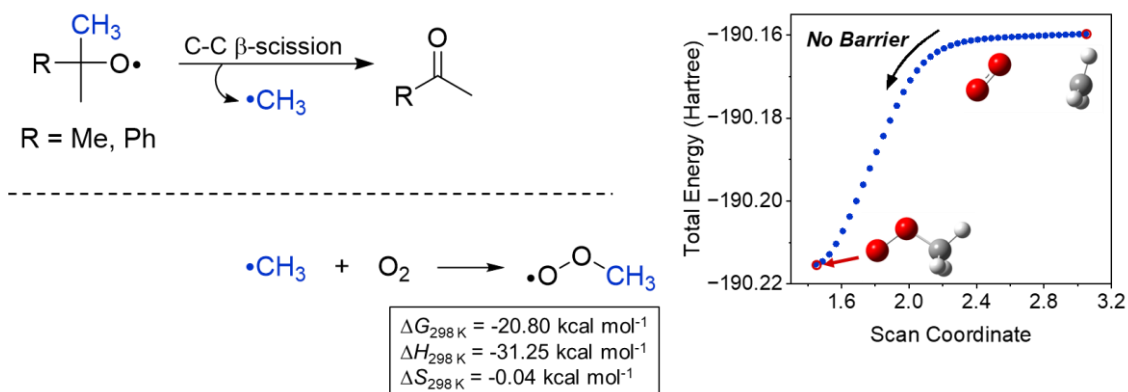
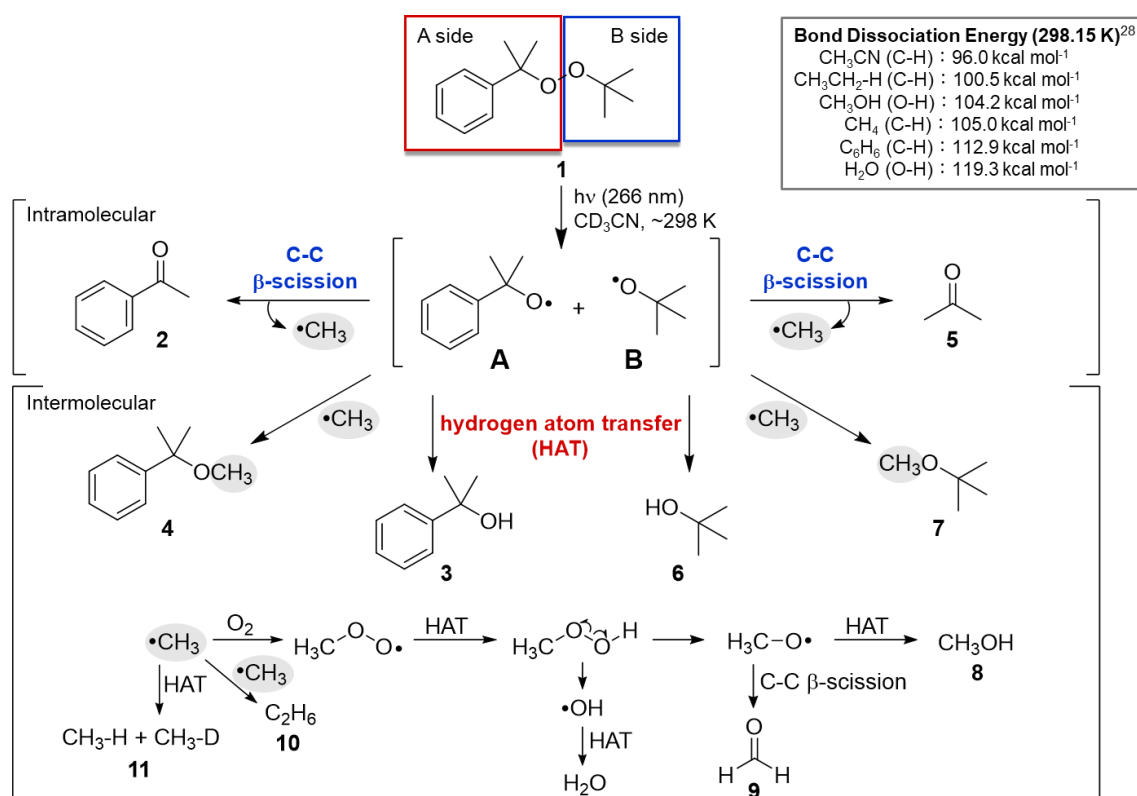


Figure 16. Generation and reactivity of methyl radical.

Scheme 2. Mechanism of the Photolysis of **1**.



2-6. Mechanism

The mechanism of the photochemical reaction in **1** is summarized in Scheme 2, which is proposed based on experimental observations of radical species by the DMPO spin trapping method and the identification and yield of photolysis products. After the

homolytic O–O bond cleavage of **1**, the radical pair of CumO• (A-side) and *t*-BuO• (B-side) are generated, which followed by the C-C β -scission reaction that leads to the production of ketones **2** and **5**, as well as •CH₃. Moreover, HAT produces corresponding alcohols **3** and **6**. The released •CH₃ reacts with the alkoxy radicals to produce ethers **4** and **7**. Once the •CH₃ is trapped by O₂, methanol (**8**) and formaldehyde (**9**) are formed after the O–O bond cleavage, from which methoxyl and hydroxyl radicals can be generated. The dimerization of •CH₃ produces ethane (**10**). Methane (**11**) can be formed by the hydrogen atom abstract from •CH₃. The deuterated isomer is formed by deuterium-atom abstraction from CD₃CN. As shown in Scheme 2, the mechanism of the formation of products in the photolysis of **1** was clarified based on the product and spectroscopic analyses.

2-7. Conclusion

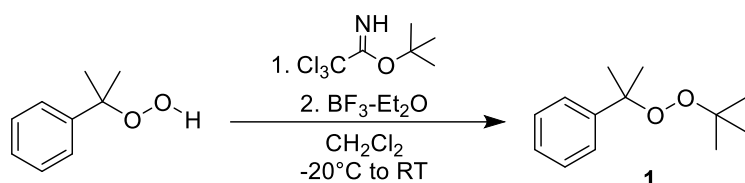
In this study, we experimentally observed two alkoxy radicals (CumO• and *t*-BuO•) generated by photoirradiation of *tert*-butyl cumyl peroxide (**1**) using the DMPO spin trapping method and investigated the structure and yield of the photoreaction products by ¹H NMR measurements. As a result, we were able to reveal information on the reactivity of the two alkoxy radicals necessary for the regulation of ROS levels in cancer cells.

2-8. Experimental Section

General Information. Materials obtained from commercial suppliers were used as received. Otherwise noted, all reactions were performed with dry solvents under an atmosphere of nitrogen gas in dried glassware. All workup and purification procedures were carried out with reagent-grade solvents under air atmosphere. Thin-layer chromatography (TLC) analyses were performed on commercial aluminum sheets of Merck silica gel 60F254 and visualized with an ultraviolet lamp ($\lambda = 254$ nm). Purification was done by column chromatography using silica gel (63-210 μ m). NMR spectra were recorded on a Bruker Ascend 400 to give ¹H NMR (400 MHz) spectra. Chemical shifts for ¹H NMR are expressed in parts per million (ppm) relative to tetramethylsilane (δ 0.00 ppm) or the residual peak of CD₃CN (δ 1.94 ppm). Data are reported as follows: chemical shift, multiplicity (s = singlet, d = doublet, dd = doublet of doublets, t = triplet), coupling constant (Hz), and integration. UV-vis spectra were recorded on a SIMADZU UV-3600 Plus spectrophotometer. High-resolution mass spectra (HRMS) were performed with a Thermo Fisher Scientific LTQ Orbitrap XL

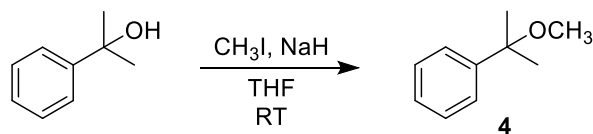
using electrospray ionization (ESI) method. EPR spectra were recorded on a Bruker BioSpin Elexsys E500.

Synthesis. *tert*-butyl cumyl peroxide (**1**).



The compound was prepared according to a known procedure.²² Added a stirring bar to the two-necked flask, drew a vacuum with drying, and purged with nitrogen. *Tert*-butyl 2,2,2-trichloroacetimidate (0.21 mL, 1.17 mmol) and a solution of cumene hydroperoxide (119.5 mg, 0.79 mmol) in CH_2Cl_2 1 mL were added to the flask, and the flask was cooled to -20°C (NaCl + ice water) with stirring. Then $\text{BF}_3-\text{Et}_2\text{O}$ diluted with CH_2Cl_2 (0.6 mL, 0.03 mmol) was dropped slowly to the reaction mixture. When the reaction temperature reached to room temperature, a small amount of NaHCO_3 was added to the reaction mixture for quenching, and solid was removed by filtration. After evaporating and purification with column chromatography (hexane/ CH_2Cl_2 = 20 : 1, R_f = 0.28), **1** (51 mg, 0.24 mmol, 19%) was obtained as colorless oil. ^1H NMR (400 MHz, CD_3CN): δ (ppm) 7.12 (d, J = 7.1 Hz, 2H), 7.24 (dd, J = 7.5, 7.5 Hz, 2H), 7.24 (t, J = 7.3 Hz, 1H), 1.53 (s, 6H), 1.21 (s, 9H). UV-vis (CH_3CN , c = 5.5 mM): λ_{max} (ϵ) = 257 (178) nm ($\text{M}^{-1} \text{cm}^{-1}$). The spectroscopic data are consistent with those reported in the literature.²⁹

Methyl Cumyl Ether (4).



The compound was prepared according to a known procedure.³⁰ NaH (60 wt% oil dispersion) (0.683 g, 17.1 mmol) was added to a two-necked-flask and the flask was purged with nitrogen. Then, THF (10 mL) was added to the flask and stirred over 30 min. To the mixture was α -cumyl alcohol dissolved in THF (3 mL) was added, and then stirred over 30 min. Finally, CH_3I was added to the reaction mixture and stirred overnight. After finished the reaction, H_2O (15 mL) was added, and then the mixture was extracted with

EtOAc. The organic layer was dried over MgSO_4 , concentrated, and purified via silica gel column chromatography (hexane/EtOAc = 5 : 1, R_f = 0.55) to obtain **4** (569 mg, 3.8 mmol, 79%) as colorless oil. ^1H NMR (400 MHz, CD_3CN): δ (ppm) 7.42 (d, J = 7.1 Hz, 2H), 7.35 (dd, J = 7.6, 6.8 Hz, 2H), 7.25 (t, J = 7.2 Hz, 1H), 3.00 (s, 3H), 1.47 (s, 6H). UV-vis (CH_3CN , c = 6.3 mM): λ_{max} (ϵ) = 257 (183) nm ($\text{M}^{-1} \text{cm}^{-1}$). The spectroscopic data are consistent with those reported in the literature.³⁰

Photoreaction. The mother solution for all photoreactions was prepared using a volumetric flask and acetonitrile- d_3 (CD_3CN , 99.9%D). 0.35 mL of the solution was added to 3-4 quartz tubes using a syringe, respectively. When the sample solution was placed under oxygen conditions, oxygen bubbling was performed for 15 minutes. The photoreactions were conducted using Nd: YAG laser (LOTIS TII: LS-2145TF) which produces 10 Hz pulse of 1 mJ at 266 nm (beam diameter: 3 cm using a beam expander lens) as light source. The distance between laser and mirror, mirror and expander lens, expander lens and quartz tube, were fixed as shown in Figure 17.

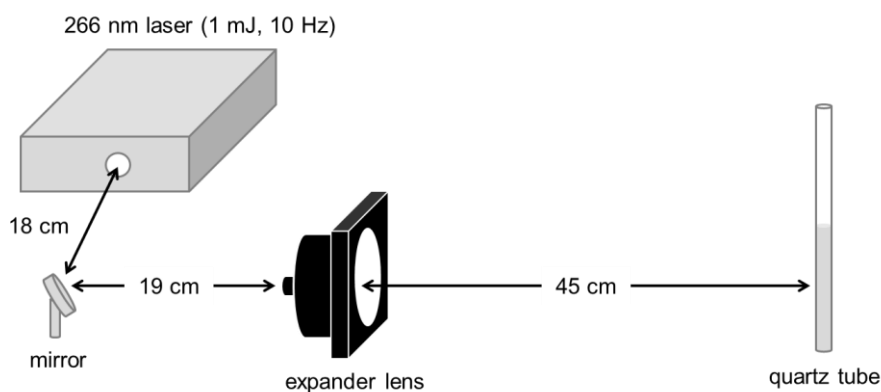


Figure 17. The distance between laser and mirror, mirror and expander lens, expander lens and quartz tube in the photoreaction of **1**.

The photoproducts were directly analyzed by ^1H NMR spectroscopy. The chemical yields of photoproducts were calculated using triphenylmethane as an internal standard. The experimental error was calculated from the results of 3-4 times photoreactions (see procedure below).

1. Photolysate after 1 h was transferred from a quartz tube into a small bottle which contains a concentration-known triphenylmethane (2 mg), and then a bottle was covered with parafilm to ultrasonicate the solution. The solution was returned into

the quartz tube, which was used in photoreaction, to measure ^1H NMR spectrum.

- From ^1H NMR spectrum of the mixture of triphenylmethane and photoreaction solution, we calculated the integral value of **1** ($2 \times \text{CH}_3$, 6H) based on that of triphenylmethane (1H), and then the amount of the unreacted **1** (mmol) was determined (Eq. 7). The conversion yield (%) of **1** was calculated from Eq. 8.

The amount of unreacted **1** (mmol) =

$$\text{The amount of triphenylmethane (mmol)} \times \text{The integral value of } \mathbf{1} \text{ after photoreaction (1H)} \quad (7)$$

The conversion yield (%) =

$$\frac{(\text{The amount of } \mathbf{1} \text{ before photoreaction} - \text{The amount of the unreacted } \mathbf{1} \text{ (mmol)})}{\text{The amount of } \mathbf{1} \text{ before photoreaction (mmol)}} \times 100 \quad (8)$$

- From ^1H NMR spectrum measured immediately after photoreaction (before opened quartz tube, without triphenylmethane), the integral values of photoproducts based on **1** (6H: 6.00) were calculated. Because the integral value of **1** was not changed before/after the addition of triphenylmethane, the integral values of photoproducts were calculated using that of **1**.
- The amount of photoproducts (mmol) and their chemical yields were calculated using Eqs. 9 and 10.

The amount of photoproduct (mmol) =

$$\text{The amount of the unreacted } \mathbf{1} \text{ (mmol)} \times \text{The integral value of photoproduct (1H)} \quad (9)$$

The chemical yield of photoproduct (%) =

$$\frac{\text{The amount of photoproduct (mmol)}}{\text{The amount of consumed } \mathbf{1} \text{ by photoreaction (mmol)*}} \times 100 \quad (10)$$

*The amount of consumed **1** by photoreaction (mmol) =

$$\text{The amount of } \mathbf{1} \text{ before photoreaction} - \text{The amount of the unreacted } \mathbf{1} \text{ (mmol)}$$

The chemical yields of photoproducts of **1** under air and O_2 conditions (three times) calculated by the above procedure are shown in Tables 6a and 6b, respectively.

Table 6a. The chemical yields of photoproducts of **1** under air atmosphere.

entry	conv /%	A-side			B-side			A/B-side				
		2	3	4	5	6	7	8	9	10^a	11	11-d
1	70.8	96.9	5.7	2.7	60.4	20.8	18.4	5.1	0.6	38.5	3.1	1.6
2	69.4	92.8	5.0	2.4	58.8	19.2	18.4	5.0	0.6	37.3	3.2	1.6
3	72.2	92.7	4.6	2.3	54.0	16.0	16.3	4.2	0.4	35.8	3.1	1.5
average	70.8	94.1	5.1	2.5	57.7	18.7	17.7	4.8	0.5	37.2	3.1	1.6
standard deviation	±1.4	±2.4	±0.6	±0.2	±3.3	±2.4	±1.2	±0.5	±0.1	±1.4	±0.1	±0.1

Table 6b. The chemical yields of photoproducts of **1** under O₂ atmosphere.

entry	conv /%	A-side			B-side			A/B-side				
		2	3	4	5	6	7	8	9	10^a	11	11-d
1	73.6	92.4	6.8	2.1	59.1	30.0	16.0	10.8	1.3	31.7	4.2	1.5
2	72.2	96.3	6.3	1.7	61.2	28.6	13.5	13.8	1.9	30.6	3.6	1.2
3	70.8	101.2	8.8	2.0	61.6	34.1	13.3	19.2	2.0	31.7	5.1	1.4
average	72.2	96.6	7.3	1.9	60.6	30.0	14.3	14.6	1.7	31.3	4.3	1.4
standard deviation	±1.4	±4.4	±1.3	±0.2	±1.3	±3.6	±1.5	±4.3	±0.4	±0.6	±0.8	±0.2

^aThe chemical yield of ethane (**10**) was calculated using Eq. 11 because **10** is generated from the dimerization of •CH₃ released from C-C β-scission of CumO• and *t*-BuO•.

The chemical yield of **10** (%) =

$$\text{The chemical yield of 10 calculated from Eq. 10 (\%)} \times \{(\text{The chemical yield of } \mathbf{2} + \mathbf{5} (\%)) \times 0.01\} \quad (11)$$

EPR Spin Trapping Experiments. All procedures were conducted under dark conditions due to the photosensitivity of 5,5-Dimethyl-1-pyrroline N-Oxide (DMPO).

The sample solution was prepared using a volumetric flask and acetonitrile (CH₃CN, Spectro grade). An aqueous flat cell was used for measuring EPR spectra of the photoreaction sample. All photoreaction measurements were performed at room temperature (~298 K) using a high-pressure Hg lamp (Hamamatsu Photonics, LIGHTNINGCURE: L9566) without a filter for generating a lot of radicals at the same time. The main emitted wavelengths are 254, 313, 365, 407, 440, and 550 nm. EPR spectra were obtained at modulation frequency: 100 kHz, smooth point: 1, number of scan: 3, modulation amplitude: 0.3 G, receiver gain: 60 dB, number of points: 16384, and sweep time: 81.92 ms.

Laser Flash Photolysis Measurements. All samples were detected at room temperature (~293 K) by Laser Flash Photolysis (LFP), using a LOTIS TII: LS-2145TF Nd: YAG laser (266 nm, ca. 7-10 mJ/pulse, 10 ns pulse-width). The monitoring system consisted of a 150 W xenon lamp as a light source, Unisoku-MD200 monochromator and a photomultiplier. The sample solution was prepared using CH₃CN (Spectro grade) and Abs was adjusted to 0.5~1.0. A 5 mm (in the direction of the laser beam) × 10 mm (in the direction of the analyzing light) quartz cell was used for LFP measurements. The fall process of CumO• was detected at 485 nm under air atmospheric conditions.

2-9. Supplementary Material

¹H NMR spectra.

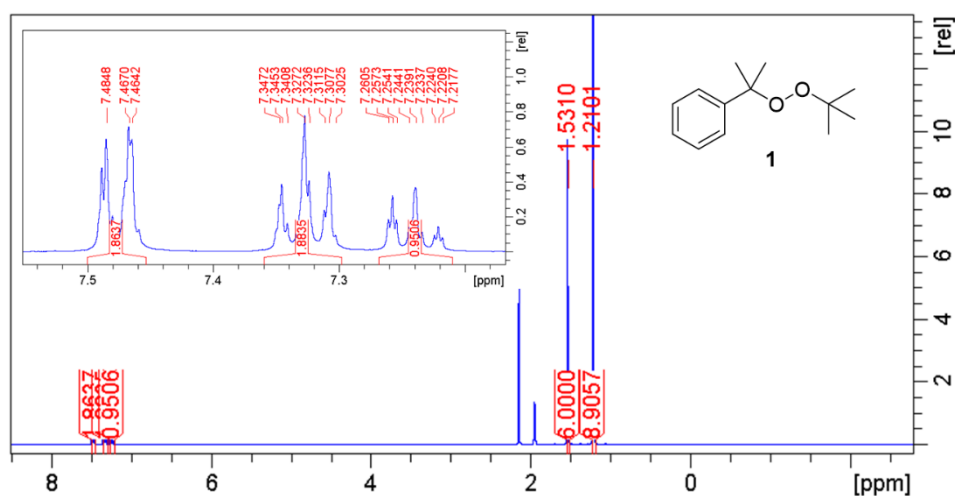


Figure 18. ¹H NMR (400 MHz, CD₃CN) spectrum of 1.

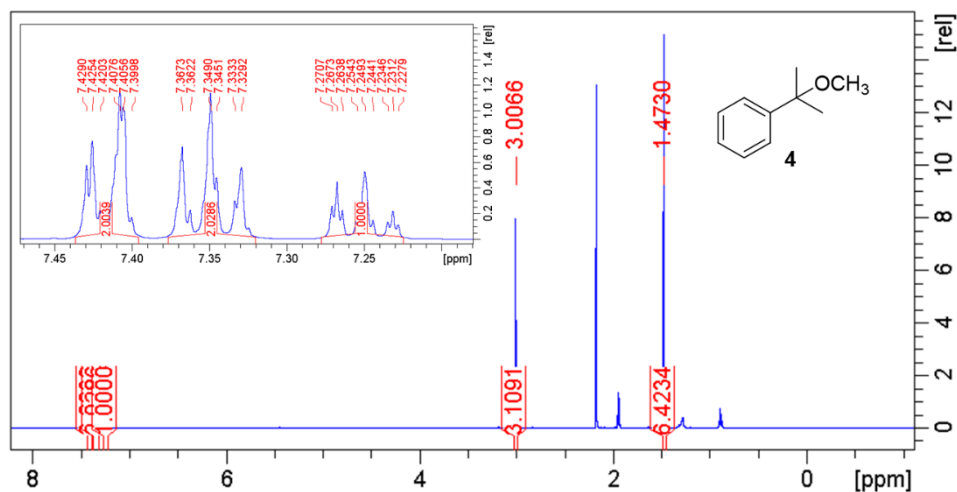
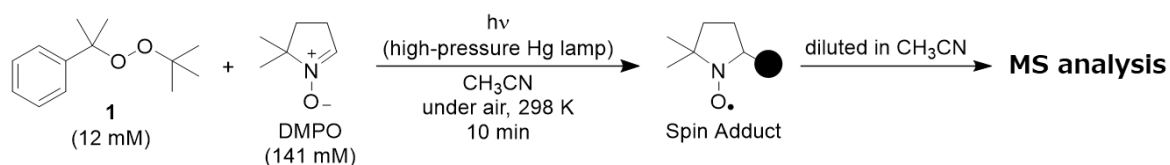


Figure 19. ¹H NMR (400 MHz, CD₃CN) spectrum of **4**.

HRMS (ESI+) spectra of spin adducts generated in the photoreaction of **1 and DMPO.** High-resolution mass spectra (HRMS) were performed with a Thermo Fisher Scientific LTQ Orbitrap XL using ionization positive (ESI+; 6 kV, capillary temperature: 100 °C) method.



Scheme 3. Method of detecting spin adducts generated in the photolysis of **1** (12 mM) in the presence of DMPO (141 mM) in acetonitrile using a high-pressure Hg lamp. The photoreaction solution was diluted in acetonitrile before conducting mass spectrometry measurements.

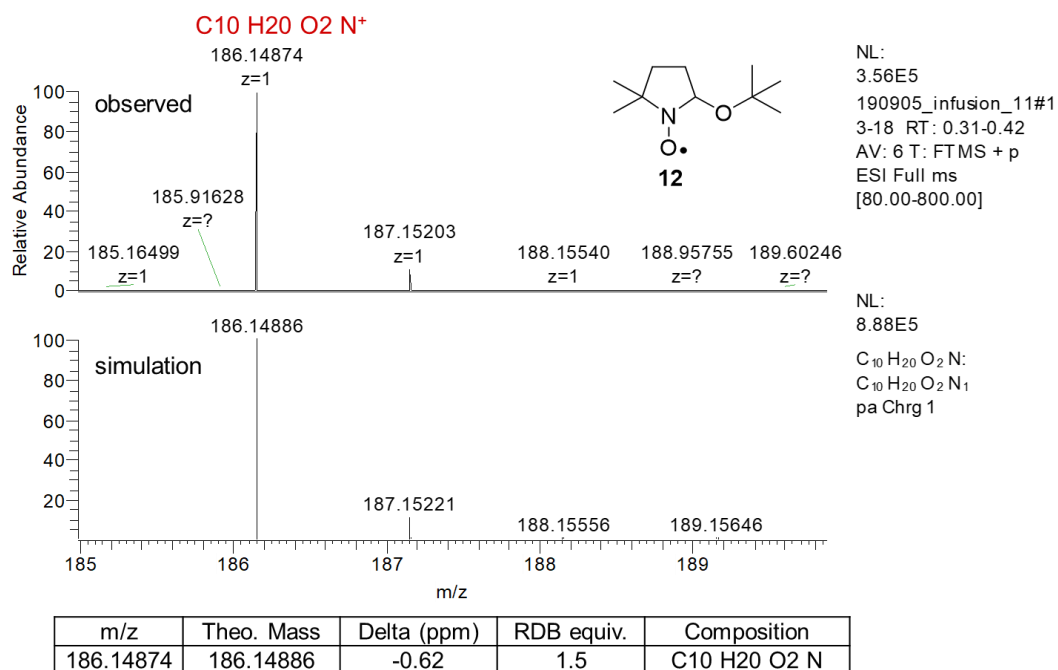


Figure 20. HRMS (ESI+) observed and simulation spectra of **12**.

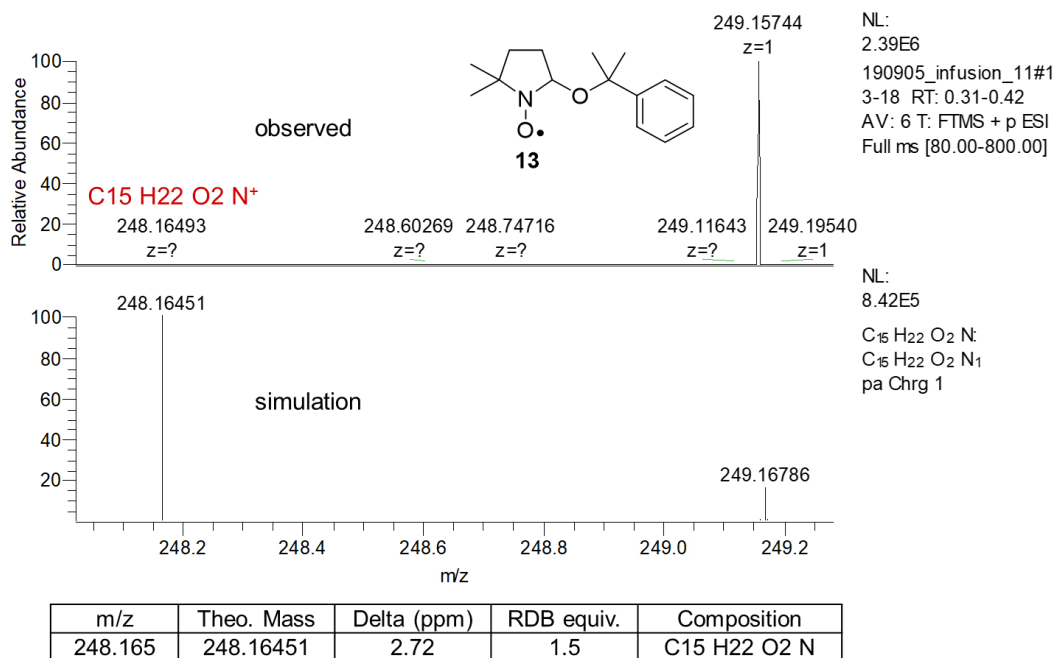


Figure 21. HRMS (ESI+) observed and simulation spectra of **13**.

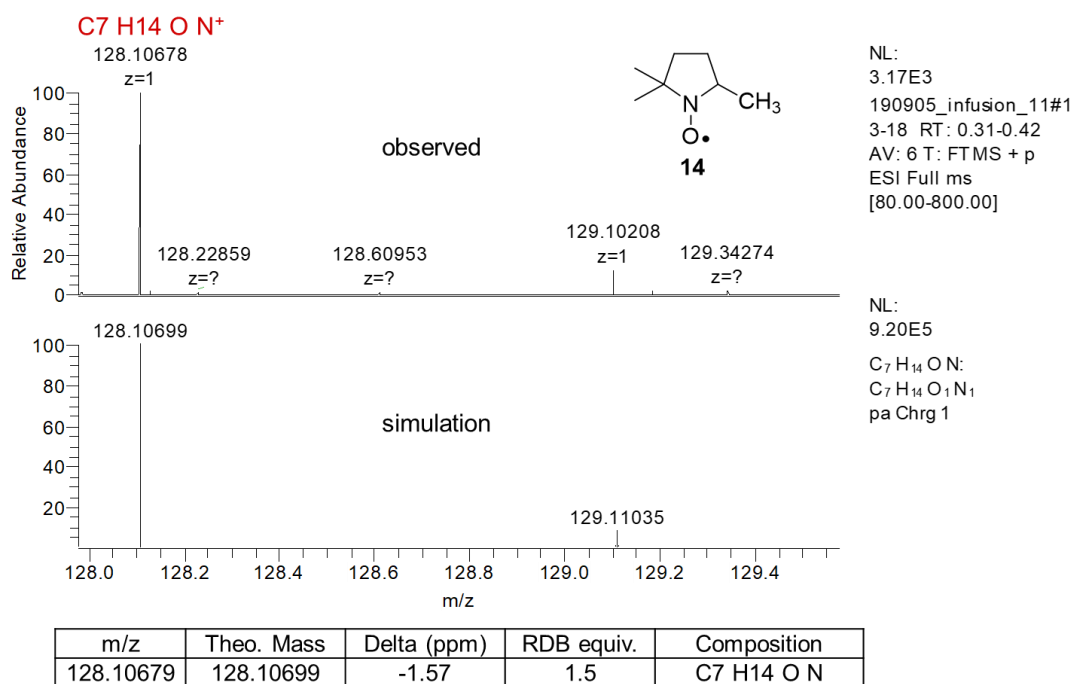


Figure 22. HRMS (ESI+) observed and simulation spectra of **14**.

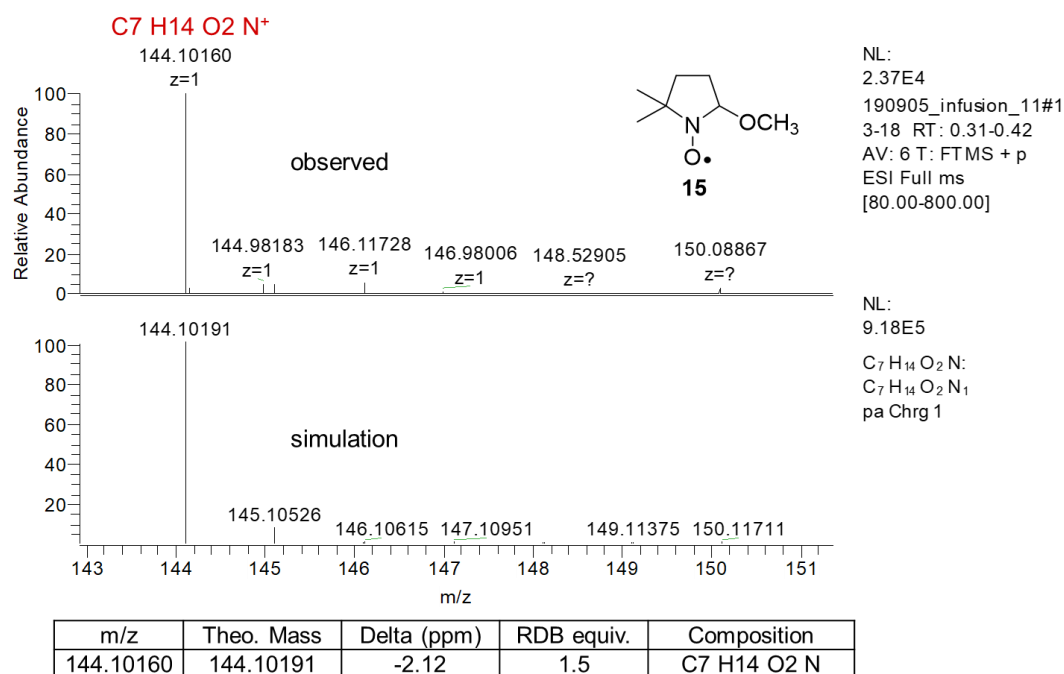


Figure 23. HRMS (ESI+) observed and simulation spectra of **15**.

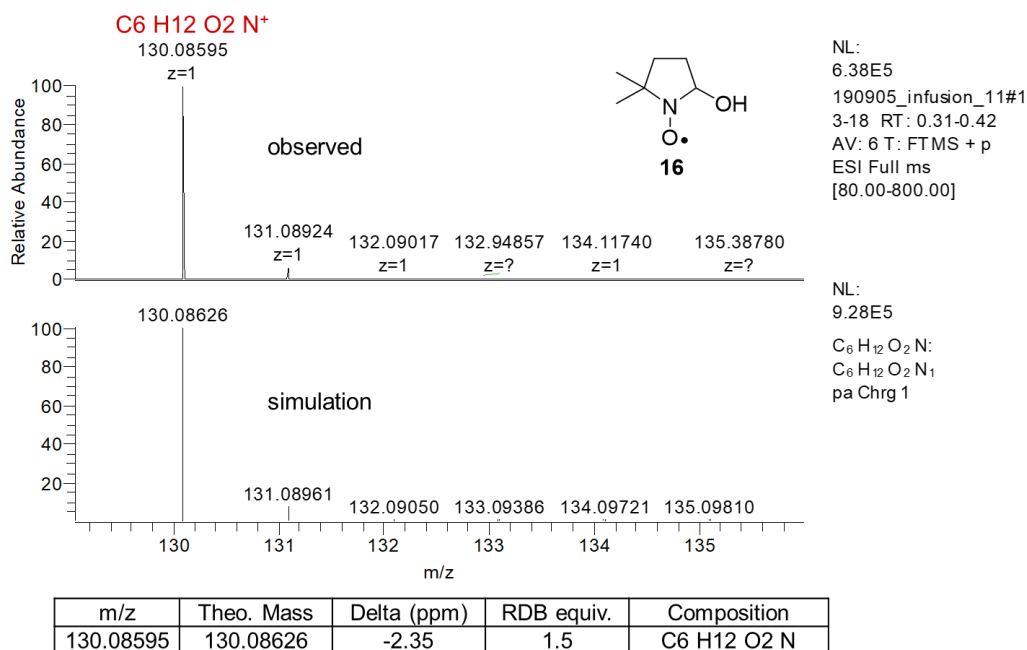


Figure 24. HRMS (ESI+) observed and simulation spectra of **16**.

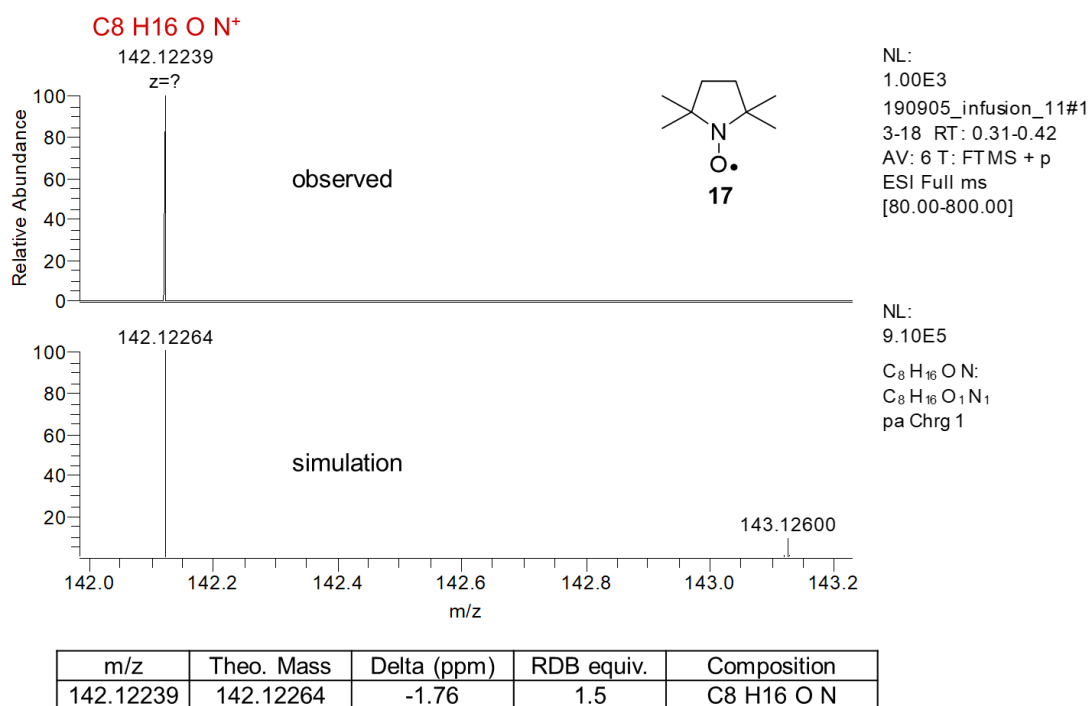


Figure 25. HRMS (ESI+) observed and simulation spectra of **17**.

Photoproducts analysis of 1 by ^1H NMR measurements. ^1H NMR spectra of **1** (blue spectrum), the photolysate after 1 h of **1** under air (green spectrum), and under O_2 (red spectrum) without triphenylmethane are shown in Figures 26a-d.

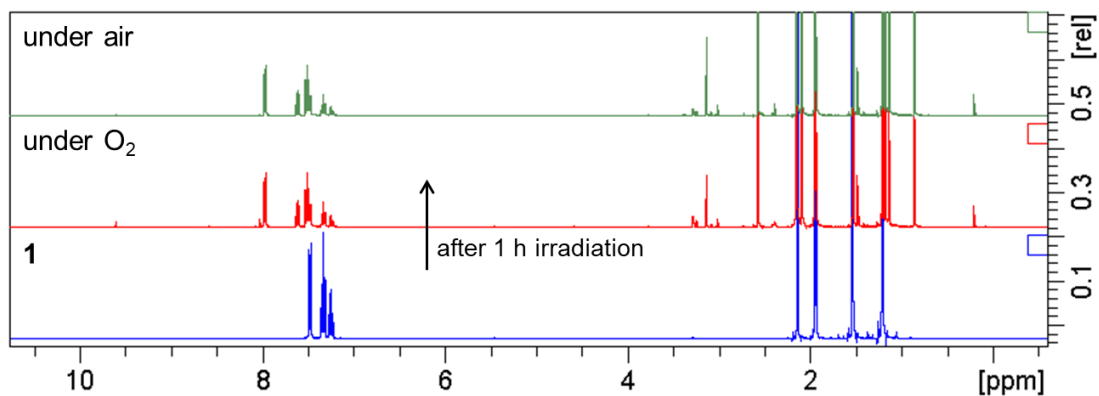


Figure 26a. ^1H NMR spectra of **1** (bottom, blue), the photolysate after 1 h of **1** under O_2 (middle, red) and under air (top, green) without triphenylmethane in CD_3CN .

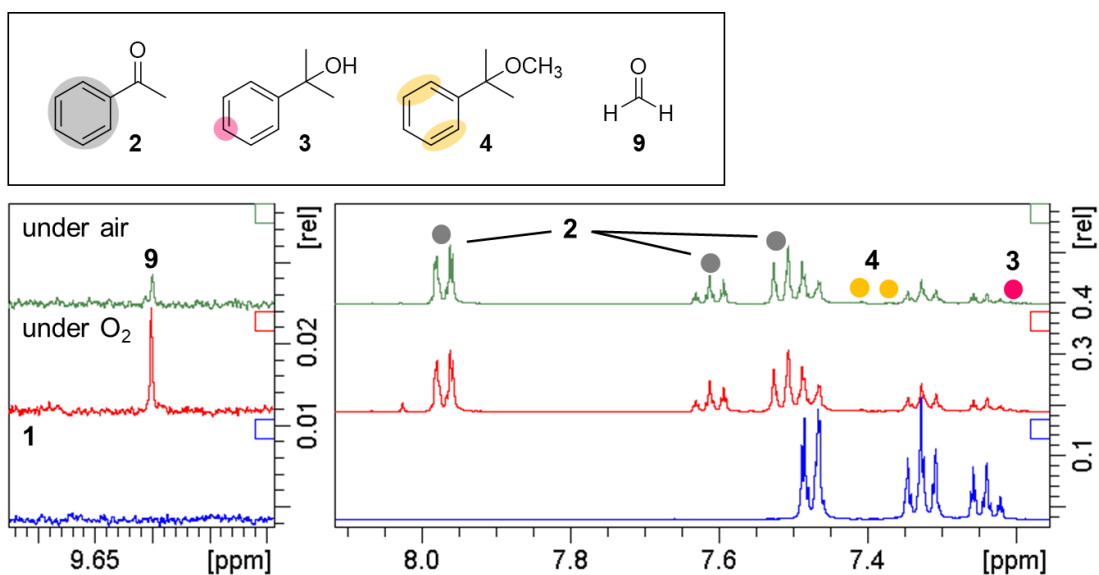


Figure 26b. Enlarged spectra of Figure 26a in the regions of 9.6 ppm and 8.1-7.2 ppm.

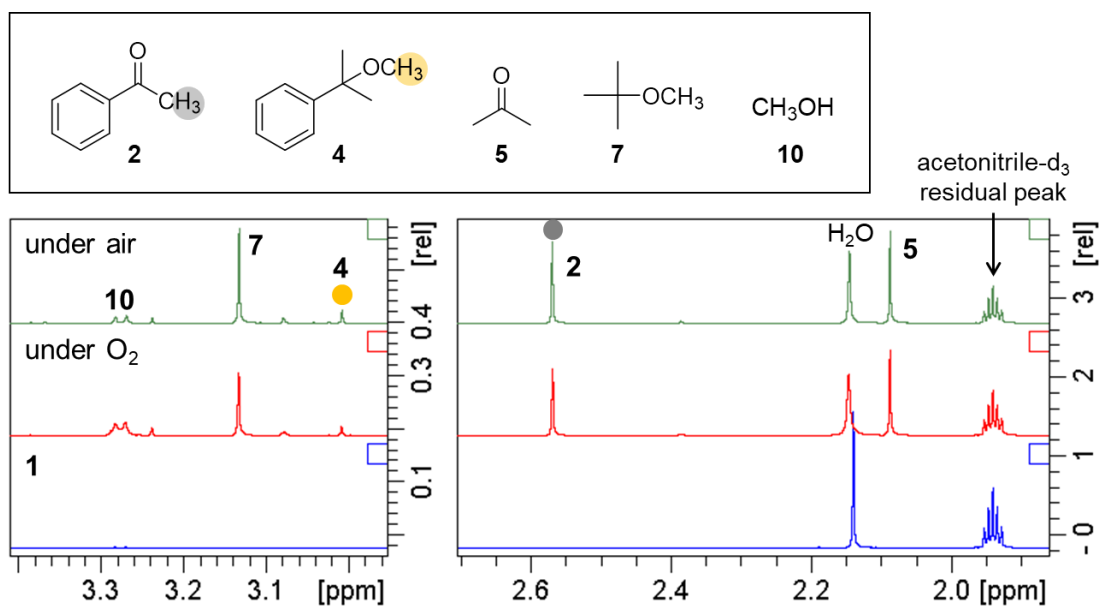


Figure 26c. Enlarged spectra of Figure 26a in the regions of 3.4-3.0 ppm and 2.7-1.9 ppm.

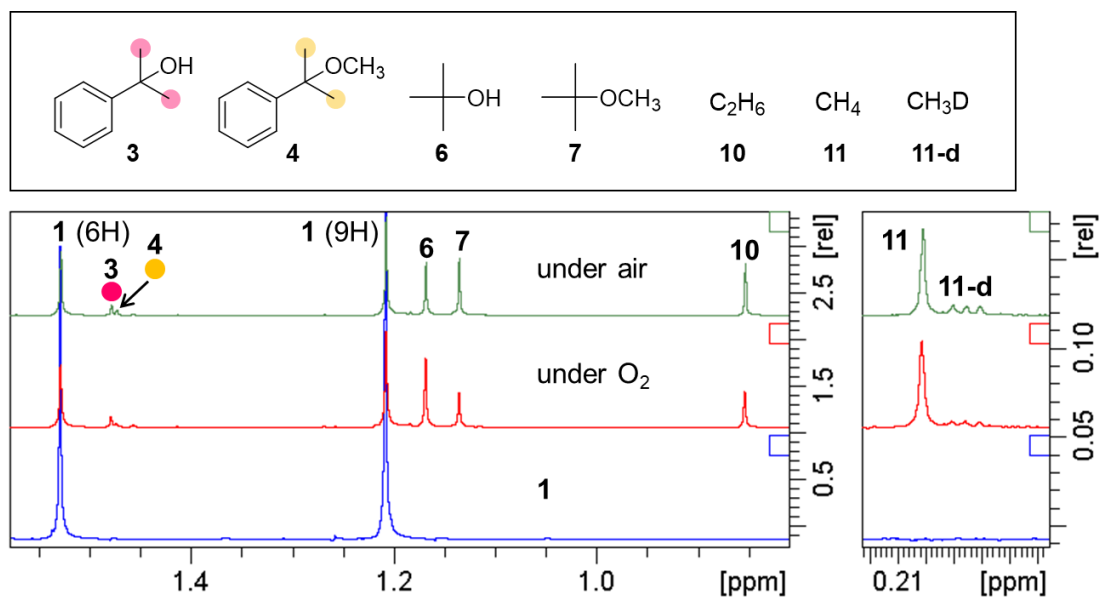


Figure 26d. Enlarged spectra of Figure 26a in the regions of 1.5-0.9 ppm and 0.2 ppm.

Chapter 3

DMPO Spin Trapping Study in the Photolysis of 2-(4-Nitrophenyl)-1*H*-indolyl-3-methyl Derivatives

3-1. Introduction

The development of photolabile protecting groups (PPGs) which protect a highly reactive functional group (X), rendering it temporarily inactive and regenerating the functional group by photoirradiation, has been actively studied because they can be regenerated without the use of external reagents such as acids or bases.³¹ In our group, we have developed a new PPGs, a 2-(4-nitrophenyl)-1*H*-indolyl-3-methyl (NPIM) derivatives containing an indole moiety, and achieved the efficient release of alcohols (X = OR), amines (X = NHR), and carboxylic acids (X = OC(O)R) by visible light irradiation (Figure 27).³² The NPIM group is advantageous because it enables the release of even poor leaving groups such as alcohols (**19c,d**) and amines (**19e,f**), giving moderate to high yields of products (Table 7). In addition, the photochemical release of X was accelerated by the presence of oxygen (Table 8, entries 2 and 3). Therefore, homolysis of the C-X was proposed to generate the corresponding radicals in the photochemical deprotection of the functional groups.

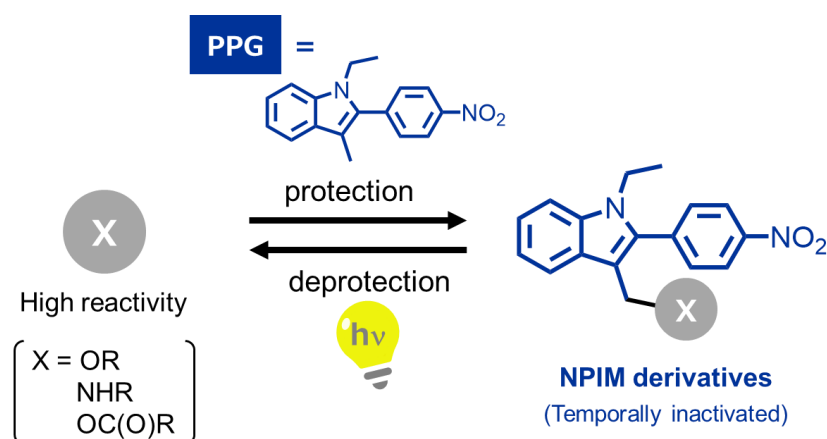
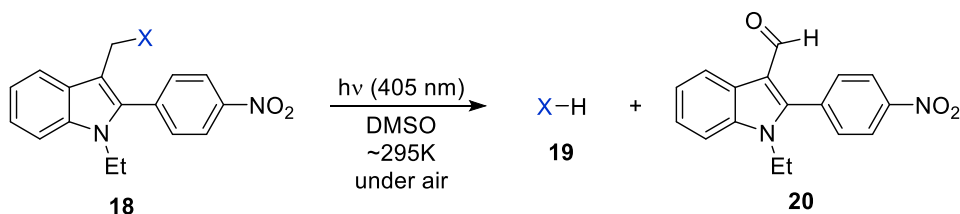


Figure 27. Photochemical release of alcohols (X = OR), amines (X = NHR), and carboxylic acids (X = OC(O)R) using NPIM derivatives.

In this study, we investigated the radical species generated in the photolysis of compound **18a** (X = OC(O)Ph). To clarify the molecular structure of the photoproducted radicals, the DMPO spin trapping method was used to detect and identify the reactive intermediate radical species by forming relatively stable spin adducts as the same method as shown in chapter 2. In this experiment, benzene, which showed the highest photoreaction efficiency in the previous study, was selected as a solvent (Table 8, entry 4).

Table 7. Photochemical release of X using NPIM derivatives.³²

entry	18 (X)	products (yields, %) ^a reaction time
1	18a (OC(O)Ph)	19a (98), 20 (36) 4 h
2	18b (OC(O)Me)	19b (86), 20 (35) 2.5 h
3	18c (OPh)	19c (95), 20 (48) 1 h
4	18d (OEt)	19d (87), 20 (65) 1 h
5	18e (NHPh)	19e (62), 20 (59) 3 h
6	18f (NHCH ₂ Ph)	19f (57), 20 (-) 3 h

^aThe yields of photoproducts were determined using ¹H NMR spectroscopy with triphenylmethane as an internal standard.

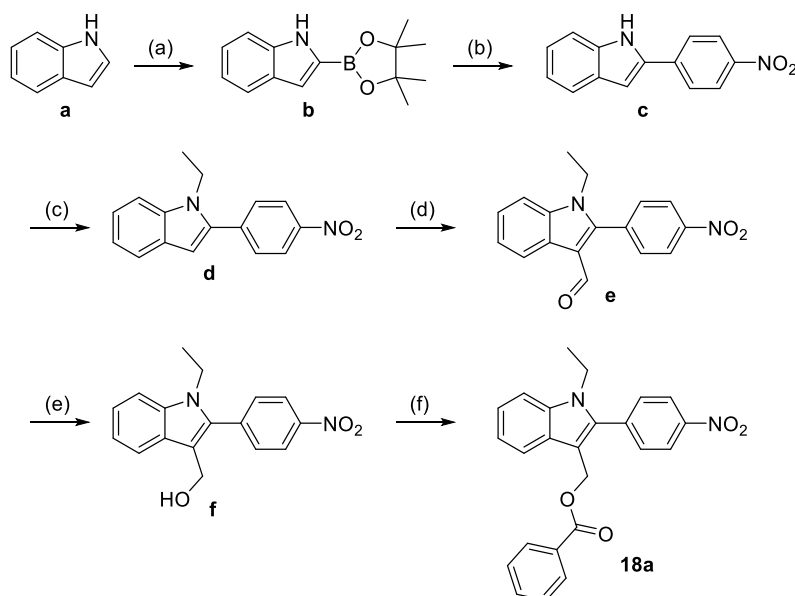
Table 8. Photolysis of **18a** under different conditions.³²

entry	solvent	conditions	reaction time (min)	yields of 19a and 20 (%)	quantum yield (%) ^a
1	DMSO- <i>d</i> ₆	under air	240	19a (98) 20 (36)	2
2	CD ₃ CN	under air	40	19a (80) 20 (26)	12
3	CD ₃ CN	under N ₂ ^b	90	19a (55) 20 (20)	5
4	C ₆ D ₆	under air	15	19a (51) 20 (16)	45
5	C ₆ D ₆ /D ₂ O (29/1) v/v	under air	25	19a (64) 20 (9)	19

^aThe quantum yields of the consumption of **18a** were determined using a ferrioxalate actinometer. ^bN₂ bubbling for 20 min.

3-2. Synthesis and Absorption spectrum of 18a

Compound **18a** was synthesized as shown in Scheme 4. UV-visible absorption spectroscopy was performed on the synthesized compound **18a** (Figure 28). Absorption bands were observed in benzene at about 300-450 nm.



Scheme 4. Synthesis of **18a**; Reagents and conditions: (a) 4,4'-Di-*tert*-butyl-2,2'-bipyridyl (dtbpy), [Ir(COD)OMe]₂, bis(pinacolato)diboron, 50°C, 18 h, 76% yield. (b) 1-Iodo-4-nitrobenzene, Pd(PPh₃)₄, K₂CO₃, 80°C, 2 h, 54% yield. (c) NaH, EtI, 0°C to RT, 18 h, 89% yield. (d) DMF, POCl₃, 0°C to RT, 3 h, 83% yield. (e) NaBH₄, RT, 1 h, 94% yield. (f) Benzoic anhydride, DMAP, 0°C to RT, 3 h, 30% yield.

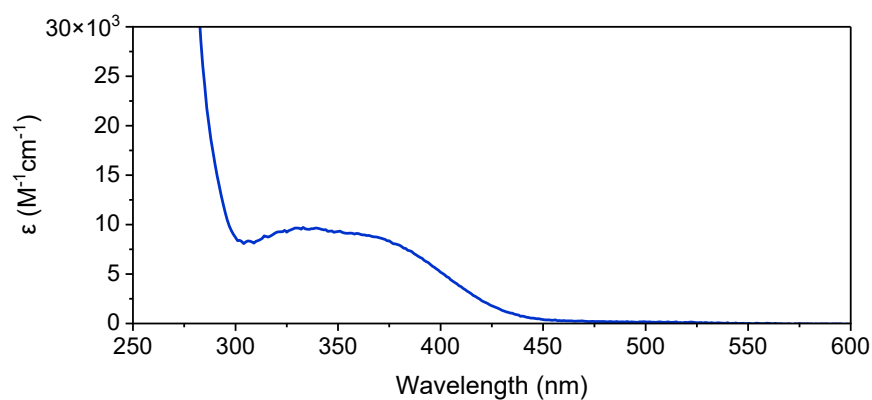


Figure 28. UV-vis absorption spectrum of **18a** in benzene.

3-3. Detection of Radical Species by Spin Trapping

First, the photoreaction of **18a** (10.7 mM) in the presence of DMPO (102.5 mM) was conducted in an EPR resonant cavity using a 365 nm LED lamp in benzene at 298 K under air atmosphere. After photoirradiation of the solution in a quartz tube, the typical EPR signals of nitroxides ($R_2N-O\cdot$) were detected (Figure 29a). EPR simulation using WinEPR simulation software²³ clarified that the EPR signals obtained in the photolysis of **18a** in the presence of DMPO corresponded to three spin adducts. The HFCC values of three spin adducts were determined to be as follows: $a_N = 12.75$ G, a_H^β

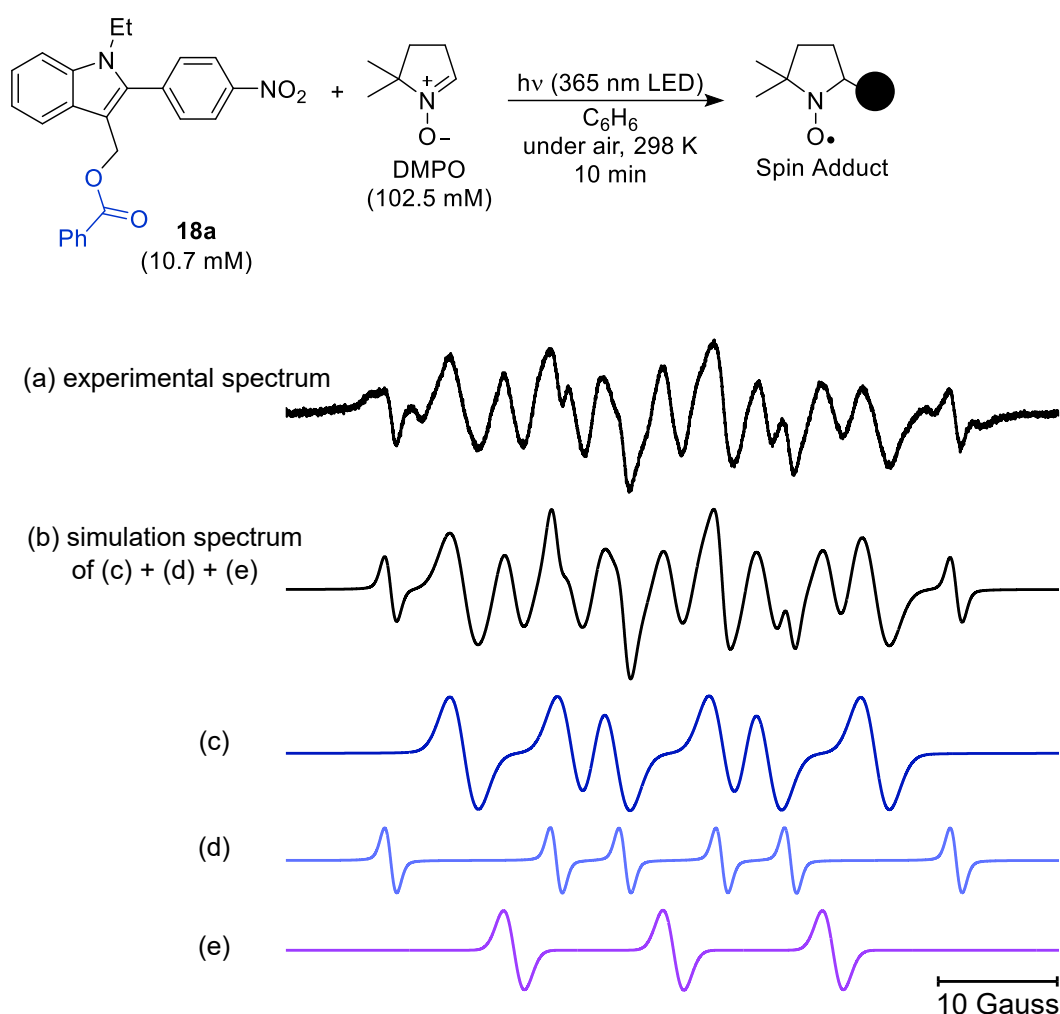


Figure 29. (a) EPR spectrum obtained after the photolysis of **18a** (10.7 mM) and DMPO (102.5 mM) in benzene using a 365 nm LED lamp. (b) Simulation spectrum of sum of (c; $a_N = 12.75$ G, $a_H^\beta = 9.04$ G), (d; $a_N = 13.92$ G, $a_H^\beta = 19.69$ G), and (e; $a_N = 13.40$ G) with at 3.8: 1: 1.8 ratio. (c)-(e) Simulation spectra.

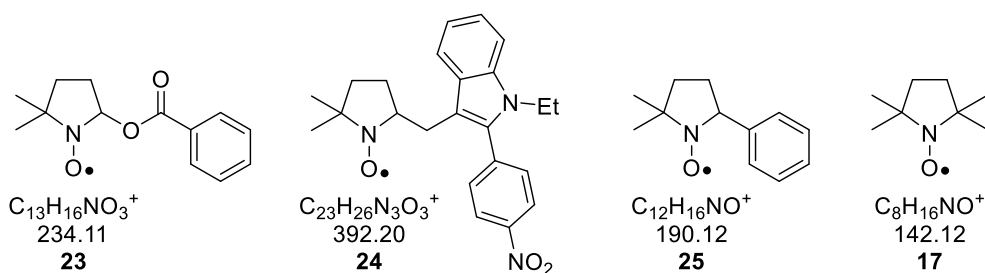


Figure 30. Spin adducts **23-25**, **17** were detected by electrospray ionization-MS (FTMS, positive mode) measurements.

= 9.04 G (Figure 29c), $a_N = 13.92$ G, $a_{H^\beta} = 19.69$ G (Figure 28d), $a_N = 13.40$ G (Figure 29e).

To obtain information about the structures of spin adducts detected in the photoreaction **18a** and DMPO, an MS analysis was conducted on the photolysate. According to the MS results, three spin adducts **23-25** were suggested to form during the photolysis of **18a** (Figure 30), indicating the formation of 2-(4-nitrophenyl)-1*H*-indoly-3-methyl radical (\bullet NPIM), benzyloxy radical (\bullet OC(O)Ph), and phenyl radical (\bullet Ph). In addition to these, the mass number corresponding to spin adduct **17**,²⁴ in which the hydrogen atom at β -position is replaced by a methyl group, was detected, with **17** assigned to the EPR spectrum in Figure 29(e).

To confirm the molecular structures of the DMPO spin adducts showing the spectra in Figures 29(c) and 29(d), the HFCC values of spin adducts **23**, **24**, and **25** were calculated by quantum chemical calculations and compared with experimental values. DMPO spin adducts **23-25** were optimized to obtain the equilibrium ring and rotational conformers at LC- ω PBE with the 6-31G(d) basis set in benzene (SMD), whose HFCC values were calculated at the same level of theory using the Gaussian 16 program.

According to the calculations using the procedure described in chapter 1, spin adducts DMPO-OC(O)Ph (**23**), DMPO-NPIM (**24**), and DMPO-Ph (**25**) have two, six, and four energetically stable conformations, respectively (Figures 31-33, Tables 9-11). The average HFCC, a_N and a_{H^β} values for each spin adduct were calculated by Eqs. 11 and 12 for spin adduct DMPO- OC(O)Ph (**23**), by Eqs. 13 and 14 for spin adduct DMPO-NPIM (**24**), and by Eqs. 15 and 16 for spin adduct DMPO-Ph (**25**).

The computed average HFCC values of the DMPO spin adducts are summarized in Table 12. The calculated HFCC values of spin adducts **23-25** were compared with the experimentally obtained HFCC values. From the correlation between experimental and

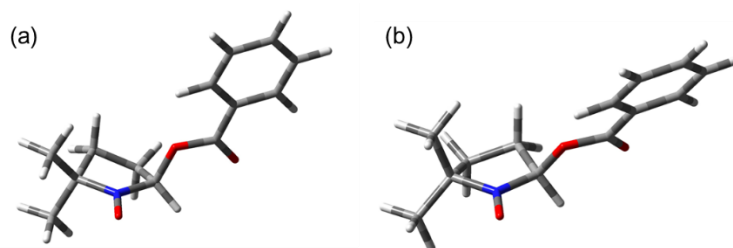


Figure 31. Two optimized conformers of spin adduct DMPO-OC(O)Ph (**23**).

Table 9. Two conformers of spin adduct DMPO- OC(O)Ph (**23**).

Conformation	Total energy (Hartree)	Relative population	a_N (Gauss)	a_H^{β} (Gauss)
(a) 4T_3	-784.909037	0.856	8.42	7.05
(b) 3T_4	-784.907357	0.144	8.99	15.23

$$a_N = (8.42 \text{ G} \times 0.856) + (8.99 \text{ G} \times 0.144) \approx 8.50 \text{ G} \quad (11)$$

$$a_H^{\beta} = (7.05 \text{ G} \times 0.856) + (15.23 \text{ G} \times 0.144) \approx 8.23 \text{ G} \quad (12)$$

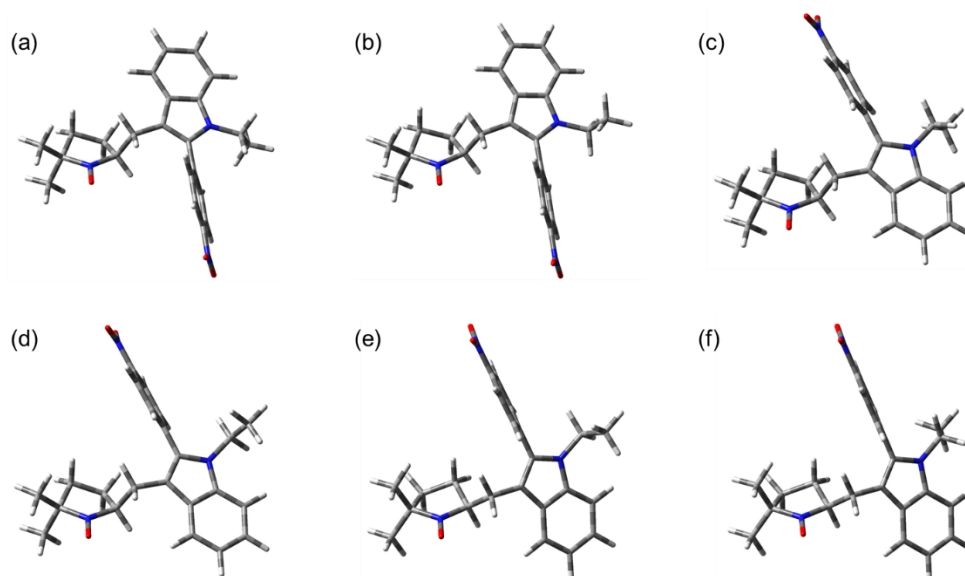


Figure 32. Six optimized conformers of spin adduct DMPO-NPIM (**24**).

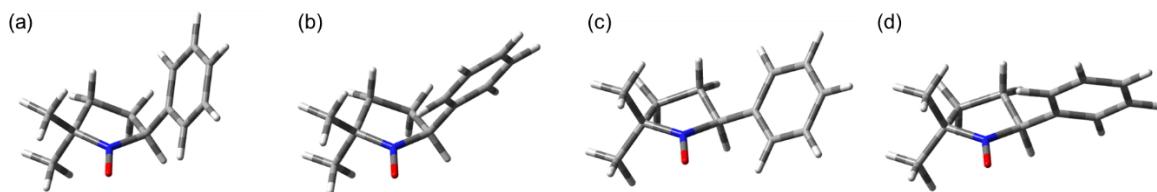
calculated HFCC values (Figures 34a,b), the spectrum in Figure 29(c) and Figure 29(d) correspond to the spin adduct **23** and **24**, respectively. Since a phenyl radical is highly

Table 10. Six conformers of spin adduct DMPO-NPIM (**24**).

	Conformation	Total energy (Hartree)	Relative population	a_N (Gauss)	a_H^{β} (Gauss)
(a)	4T_3	-1281.079208	0.029	9.92	13.55
(b)	4T_3	-1281.079717	0.050	9.93	13.60
(c)	4T_3	-1281.080519	0.117	9.97	13.80
(d)	4T_3	-1281.080966	0.189	9.94	13.73
(e)	3T_4	-1281.081649	0.389	10.13	22.57
(f)	3T_4	-1281.081136	0.226	10.13	22.62

$$a_N = (9.92 \text{ G} \times 0.029) + (9.93 \text{ G} \times 0.050) + (9.97 \text{ G} \times 0.117) + (9.94 \text{ G} \times 0.189) + (10.13 \text{ G} \times 0.389) + (10.13 \text{ G} \times 0.226) \approx 10.06 \text{ G} \quad (13)$$

$$a_H^{\beta} = (13.55 \text{ G} \times 0.029) + (13.60 \text{ G} \times 0.050) + (13.80 \text{ G} \times 0.117) + (13.73 \text{ G} \times 0.189) + (22.57 \text{ G} \times 0.389) + (22.62 \text{ G} \times 0.226) \approx 19.18 \text{ G} \quad (14)$$

**Figure 33.** Four optimized conformers of spin adduct DMPO-Ph (**25**).**Table 10.** Six conformers of spin adduct DMPO-NPIM (**24**).

	Conformation	Total energy (Hartree)	Relative population	a_N (Gauss)	a_H^{β} (Gauss)
(a)	4T_3	-596.451015	0.075	10.12	12.58
(b)	4T_3	-596.452550	0.383	10.01	12.06
(c)	3T_4	-596.449834	0.022	11.78	21.29
(d)	3T_4	-596.452840	0.520	10.02	22.01

$$a_N = (10.12 \text{ G} \times 0.075) + (10.01 \text{ G} \times 0.383) + (11.78 \text{ G} \times 0.022) + (10.02 \text{ G} \times 0.520) \approx 10.06 \text{ G} \quad (15)$$

$$a_H^{\beta} = (12.58 \text{ G} \times 0.075) + (12.06 \text{ G} \times 0.383) + (21.29 \text{ G} \times 0.022) + (22.01 \text{ G} \times 0.520) \approx 17.47 \text{ G} \quad (16)$$

Table 12. Calculated HFCC values of the DMPO spin adducts based on ULC- ω PBE/6-31G(d) (SMD: benzene) and HFCC values analyzed from EPR measurements in the photolysis of **18a** (10.7 mM) and DMPO (102.5 mM) in benzene.

		23	24	25
Exp.	a_N	12.75	13.92	(13.76 ^a)
	a_{H^β}	9.04	19.69	(19.22 ^a)
Calc.	a_N	8.50	10.06	10.06
	a_{H^β}	8.23	19.18	17.47

^aThe HFCC values of spin adduct **25** in parentheses are the reported values in benzene.^{7a}

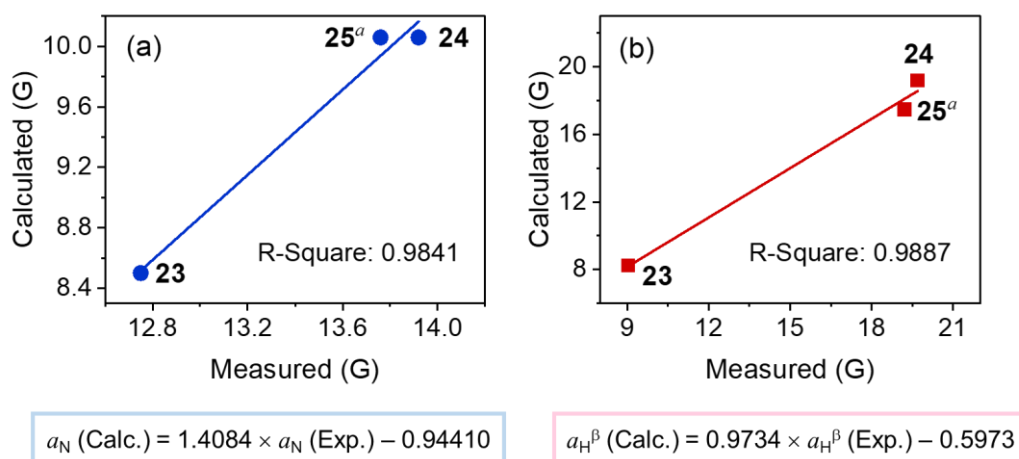


Figure 34. HFCC values of (a) nitrogen (a_N) and (b) β -hydrogen (a_{H^β}) in DMPO spin adducts in benzene. ^aThe experimental HFCC values of spin adduct **25** are the reported values in benzene.^{7a}

reactive, the concentration of spin adduct DMPO-Ph (**25**) is too low to be detected by EPR measurements in the photolysis of **18a** in the presence of DMPO. Similar EPR results were observed in the photolysis of benzoyl peroxide (10.7 mM) in the presence of DMPO (101.3 mM) (Figure 42). In Figures 34a,b, although there are only three data points for comparing the experimental and calculated HFCC values, the least square fittings, $a_N (\text{Calc.}) = 1.4084 \times a_N (\text{Exp.}) - 9.4410$ (R-squared value is 0.9841; Figure 34a) and $a_{H^\beta} (\text{Calc.}) = 0.9734 \times a_{H^\beta} (\text{Exp.}) - 0.5973$ (R-squared value is 0.9887; Figure 34b), indicated good correlations.

The photoreaction of **18a** (10.0 mM) and DMPO (100.3 mM) was also conducted using a 405 nm LED lamp as a light source (Figure 35). After the photoirradiation of the

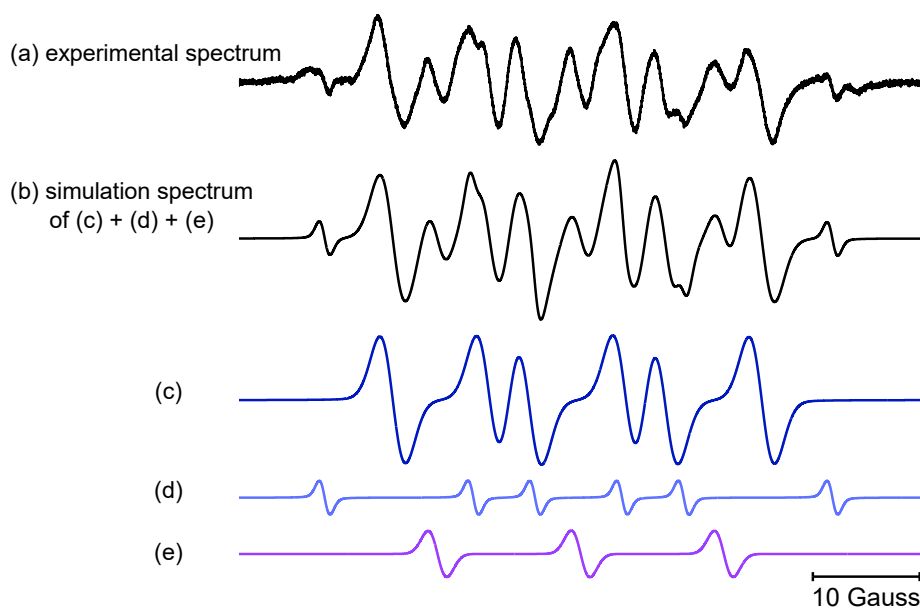
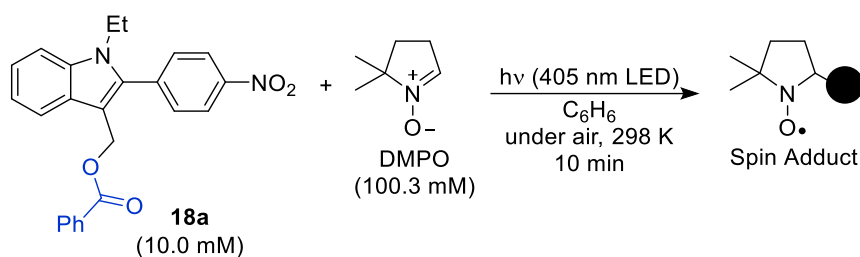


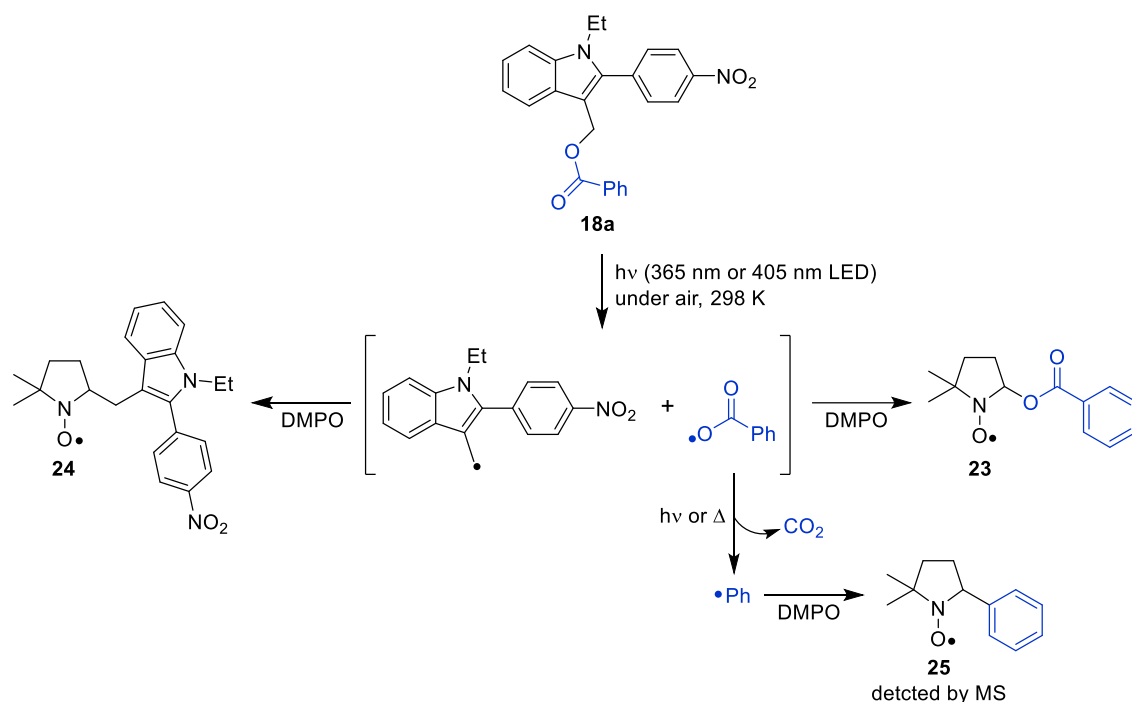
Figure 35. (a) EPR spectrum obtained after the photolysis of **18a** (10.0 mM) and DMPO (100.3 mM) in benzene using a 405 nm LED lamp. (b) Simulation spectrum of sum of (c; $a_N = 12.75$ G, $a_{H^\beta} = 9.04$ G), (d; $a_N = 13.92$ G, $a_{H^\beta} = 19.69$ G), and (e; $a_N = 13.40$ G) with at 8.2: 1: 2.1 ratio. (c)-(e) Simulation spectra.

benzene solution in a quartz tube at 298 K under air conditions, spin adducts **23**, **24**, and **17** were observed by EPR measurements, as detected in the photolysis using a 365 nm LED lamp (Figure 29). These results suggested that the photochemical decomposition of **18a** occurred homolytically to generate the radical species.

3-4. Mechanism

The mechanism of the photochemical reaction of **18a** in the presence of DMPO, which is clarified from the spin trapping experimental results, is summarized in Scheme 5. After the electronic excitation of **18a**, homolysis occurs to produce the radical pair of

Scheme 5. Mechanism of the photolysis of **18a** in the presence of DMPO.



•NPIM and •OC(O)Ph. Both radicals are captured by DMPO to form spin adducts DMPO-OC(O)Ph (**23**) and DMPO-NPIM (**24**). The benzoyloxy radical •OC(O)Ph decomposed to release CO_2 and •Ph by photoirradiation or heat;³³ the latter is trapped by DMPO to form spin adduct DMPO-Ph (**25**).

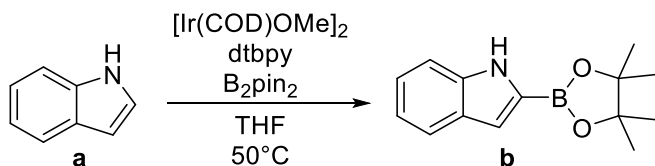
3-5. Conclusion

In this study, the structure of the radicals generated in the photolysis of **18a** was investigated by the DMPO spin trapping method. The DMPO spin trapping experimental results clarified that the generation of •NPIM and •OC(O)Ph in the photocleavage of **18a**, suggesting that the photochemical decomposition of the NPIM derivatives occurs homolytically to release alcohols, amines, and carboxylic acids.

3-6. Experimental Section

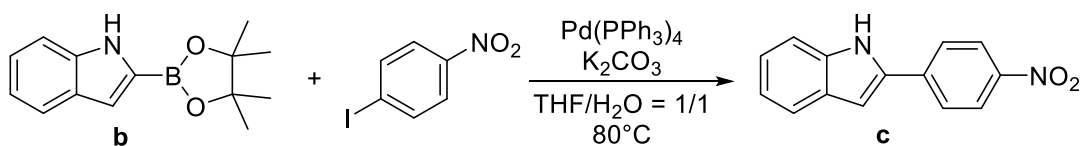
General Information. All commercially available reagents were purchased from TCI and Wako without further purification. Electron paramagnetic resonance (EPR) spectra were recorded on a Bruker BioSpin Elexsys E500. High-resolution mass spectra (HRMS) were performed with a Thermo Fisher Scientific LTQ Orbital XL using electrospray ionization positive (ESI+; 8 kV, capillary temperature: 100°C) method. NMR spectra were recorded on a Bruker Ascend 400 to give ^1H NMR (400 MHz) spectra. Chemical shifts for ^1H NMR are expressed in parts per million (ppm) relative to the residual peak of CDCl_3 (7.26 ppm). Data are reported as follows: chemical shift, multiplicity (s = singlet, d = doublet, dd = doublet of doublets, ddd = doublet of doublet of doublets, t = triplet, q = quartet, br = broad signal, m = multiplet), coupling constant (Hz), and integration. UV-vis absorption spectrum was recorded on a SIMADU UV-3600 Plus spectrophotometer.

Synthesis. 2-(4,4,5,5-Tetramethyl-1,3,2-dioxaborolan-2-yl)-1*H*-indole (**b**).³⁴



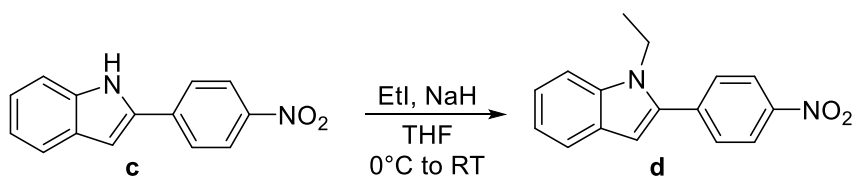
Added a stirring bar to the two-neck flask, drew vacuum with drying, and purged with nitrogen. 4,4'-Di-*tert*-butyl-2,2'-bipyridyl (dtbpy) (457 mg, 1.7 mmol), $[\text{Ir}(\text{COD})\text{OMe}]_2$ (56 mg, 0.085 mmol), bis(pinacolato)diboron (4.3 g, 17 mmol), and THF (34 mL) were added to the flask. The reaction mixture was stirred at 50°C for 10 min. After the reaction solution was turned to red dark color, indole (**a**) (4.0 g, 34 mmol) was added to the mixture, and the reaction mixture was refluxed at 50°C for 18 h. After completion of the reaction, the solvent was removed under vacuum and the product **b** was purified by short column chromatography (DCM) and gel permeation chromatography (6.3 g, 76%). ^1H NMR (400 MHz, CDCl_3): δ (ppm) 8.53 (br, 1H), 7.67 (dd, $J = 8.0, 0.8$ Hz, 1H), 7.38 (dd, $J = 8.2, 0.8$ Hz, 1H), 7.23 (ddd, $J = 8.2, 7.0, 1.1$ Hz, 1H), 7.12-7.07 (m, 2H), 1.37 (s, 12H). The spectroscopic data are consistent with those reported in the literature.³²

2-(4-Nitrophenyl)-1*H*-indole (**c**).



Added a stirring bar to the two-neck flask, drew vacuum with drying, and purged with nitrogen. **b** (5.5 g, 22.5 mmol), 1-iodo-4-nitrobenzene (3.7 g, 15.0 mmol), Pd(PPh₃)₄ (870 mg, 0.75 mmol), K₂CO₃ (2.9 g, 21.0 mmol), and THF/H₂O = 1/1 (100 mL) were added to the flask. The reaction mixture was refluxed at 80°C for 2 h. After completion of the reaction, a saturated NH₄Cl aqueous solution was added for quenching. To the crude residue was added EtOAc, followed by washing with brine water. The organic layer was collected, dried over MgSO₄, and evaporated under vacuum to yield crude, which was purified by column chromatography (hexane/EtOAc = 7:1) and recrystallization (2.9 g, 54%). ¹H NMR (400 MHz, CDCl₃): δ (ppm) 8.42 (br, 1H), 8.31 (d, *J* = 9.0 Hz, 2H), 7.80 (d, *J* = 9.0 Hz, 2H), 7.67 (d, *J* = 7.4 Hz, 1H), 7.44 (dd, *J* = 8.2, 0.8 Hz, 1H), 7.28 (ddd, *J* = 8.1, 7.1, 1.1 Hz, 1H), 7.17 (ddd, *J* = 7.9, 7.1, 1.1 Hz, 1H), 7.03 (dd, *J* = 2.1, 0.8 Hz, 1H). The spectroscopic data are consistent with those reported in the literature.³²

1-Ethyl-2-(4-nitrophenyl)-1*H*-indole (**d**).³⁵



NaH (60 wt % oil dispersion) (77 mg, 1.95 mmol) was added to a two-neck flask, and the flask was purged with nitrogen. Then, THF (2 mL) was added to the flask and stirred at room temperature for 30 min. To the mixture, **c** (294 mg, 1.3 mmol) dissolved in THF (4 mL) was added at 0°C and then stirred at rt for 30 min. Finally, EtI (0.15 mL, 1.95 mmol) was added at 0°C to the reaction mixture and stirred at room temperature for 18 h. After the reaction was complete, H₂O was added and then the mixture was extracted with EtOAc. The organic layer was dried over MgSO₄, concentrated, and purified via silica gel column chromatography (hexane/EtOAc = 20:1) to obtain **d** (260 mg, 89%). ¹H NMR (400 MHz, CDCl₃): δ (ppm) 8.34 (d, *J* = 8.9 Hz, 2H), 7.70-7.66 (m, 3H), 7.43 (dd, *J* = 8.3, 0.7 Hz, 1H), 7.30 (ddd, *J* = 8.2, 7.0, 1.1 Hz, 1H), 7.17 (ddd, *J* =

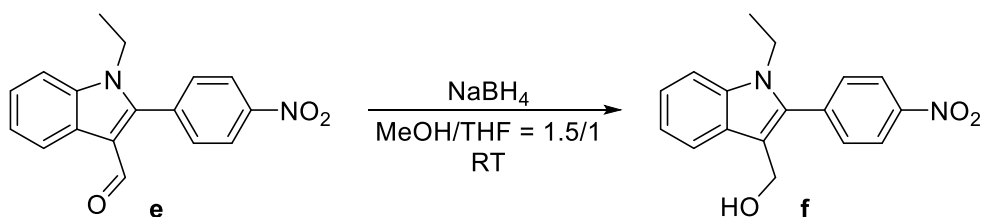
7.9, 7.0, 0.9 Hz, 1H), 6.67 (s, 1H), 4.24 (q, $J = 7.2$ Hz, 2H), 1.35 (t, $J = 7.2$ Hz, 3H). The spectroscopic data are consistent with those reported in the literature.³²

1-Ethyl-2-(4-nitrophenyl)-1*H*-indole-3-carboxaldehyde (**e**).



Added a stirring bar to the two-neck flask, drew vacuum with drying, and purged with nitrogen. Dry DMF (1.8 mL) was added to the flask, and then POCl₃ (0.12 mL, 1.3 mmol) was dropped slowly into the reaction mixture at 0°C. When the reaction temperature reached to room temperature, stirred for 15 min, and then **d** (233 mg, 0.87 mmol) dissolved in dry DMF (0.9 mL) was dropped slowly at the mixture at 0°C. The reaction mixture was stirred at room temperature for 3 h. After the reaction was complete, ice water and 1M NaOH aqueous solution were added until the reaction solution comes to pH 6-8 to afford the desired product **e** as a precipitate that was collected using vacuum filtration (213 mg, 83%). ¹H NMR (400 MHz, CDCl₃): δ (ppm) 9.72 (s, 1H), 8.46-8.42 (m, 3H), 7.72 (d, $J = 8.8$ Hz, 2H), 7.48-7.37 (m, 3H), 4.13 (q, $J = 7.2$ Hz, 2H), 1.36 (t, $J = 7.2$ Hz, 3H). The spectroscopic data are consistent with those reported in the literature.³²

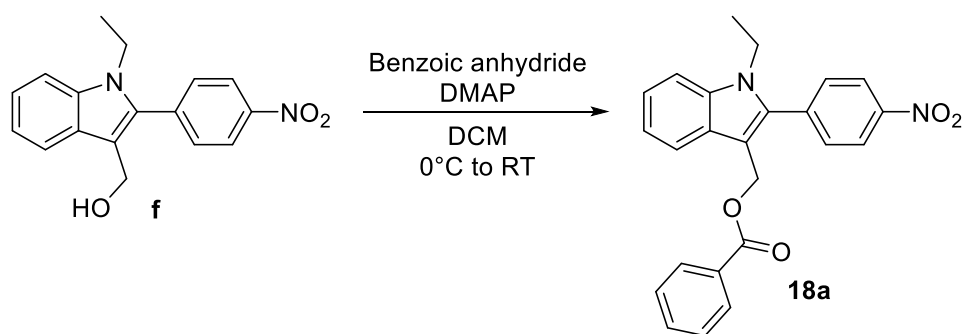
(1-Ethyl-2-(4-nitrophenyl)-1*H*-indole-3-yl)methanol (**f**).



e (101 mg, 0.34 mmol) and MeOH/THF = 1.5/1 (6.3 mL) were added to a two-neck flask, and NaBH₄ (15 mg, 0.14 mmol) was slowly added to the reaction mixture at room temperature, and then the flask was purged with nitrogen. The reaction mixture was stirred at room temperature for 1 h. After completion of the reaction, water was added for quenching at 0°C. To the crude residue was added EtOAc, followed by washing with

brine water. The organic layer was collected, dried over MgSO₄, and evaporate under vacuum to yield crude, which was purified by recrystallization (94 mg, 94%). ¹H NMR (400 MHz, CDCl₃): δ (ppm) 8.38 (d, *J* = 8.8 Hz, 2H), 7.80 (d, *J* = 7.8 Hz, 1H), 7.68 (d, *J* = 8.8 Hz, 2H), 7.43 (d, *J* = 8.2 Hz, 1H), 7.33 (ddd, *J* = 8.2, 7.0, 1.2 Hz, 1H), 7.24 (ddd, *J* = 7.9, 7.0, 1.0 Hz, 1H), 4.74 (d, *J* = 4.8 Hz, 2H), 4.14 (q, *J* = 7.2 Hz, 2H), 1.50 (t, *J* = 5.0 Hz, 1H), 1.27 (t, *J* = 7.2 Hz, 3H). The spectroscopic data are consistent with those reported in the literature.³²

(1-Ethyl-2-(4-nitrophenyl)-1*H*-indole-3-yl)methyl benzoate (**18a**).³⁶



f (60 mg, 0.20 mmol), DMAP (49 mg, 0.40 mmol), and DCM (1 mL) were added to a two-neck flask, and the flask was purged with nitrogen. To the reaction mixture was added benzoic anhydride (68 mg, 0.30 mmol) at 0°C with stirring. The reaction mixture was stirred at room temperature for 3 h under dark conditions. After completion of the reaction, a saturated NaHCO₃ aqueous solution (1 mL) was added for quenching. To the crude residue was added DCM, followed by washing with brine water. The organic layer was collected, dried over Na₂SO₄, and evaporated under vacuum to yield crude, which was purified by column chromatography (hexane/EtOAc = 10:1 with 0.1 v% Et₃N) and recrystallization (23 mg, 30%). ¹H NMR (400 MHz, CDCl₃): δ (ppm) 8.38 (d, *J* = 8.8 Hz, 2H), 8.00 (d, *J* = 7.0 Hz, 2H), 7.85 (d, *J* = 7.9 Hz, 1H), 7.69 (d, *J* = 8.8 Hz, 2H), 7.53 (t, *J* = 7.4 Hz, 1H), 7.45-7.38 (m, 3H), 7.34 (ddd, *J* = 8.2, 7.0, 1.1 Hz, 1H), 7.25 (ddd, *J* = 7.9, 7.1, 0.9 Hz, 1H), 5.44 (s, 2H), 4.13 (q, *J* = 7.2 Hz, 2H), 1.30 (t, *J* = 7.2 Hz, 3H). UV-vis (C₆H₆, c = 0.012 mM): λ_{max} (ε) = 333 (M⁻¹ cm⁻¹). The spectroscopic data are consistent with those reported in the literature.³²

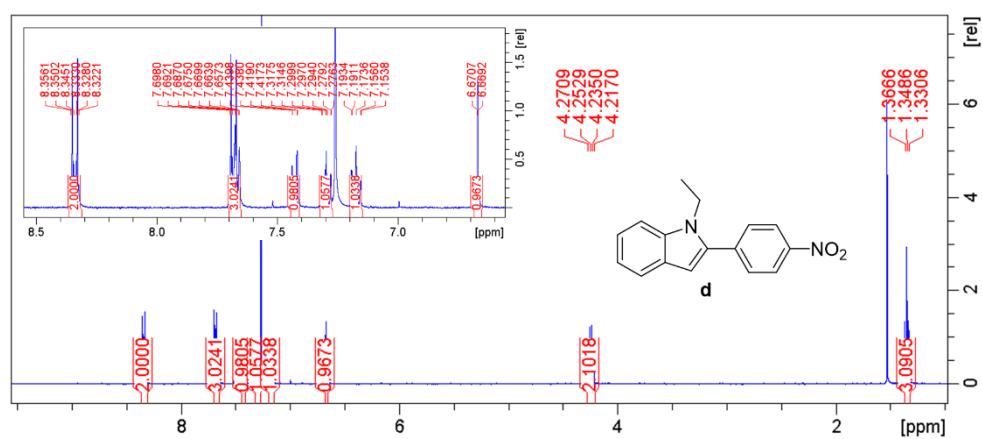


Figure 38. ¹H NMR (400 MHz, CDCl₃) spectrum of **d**.

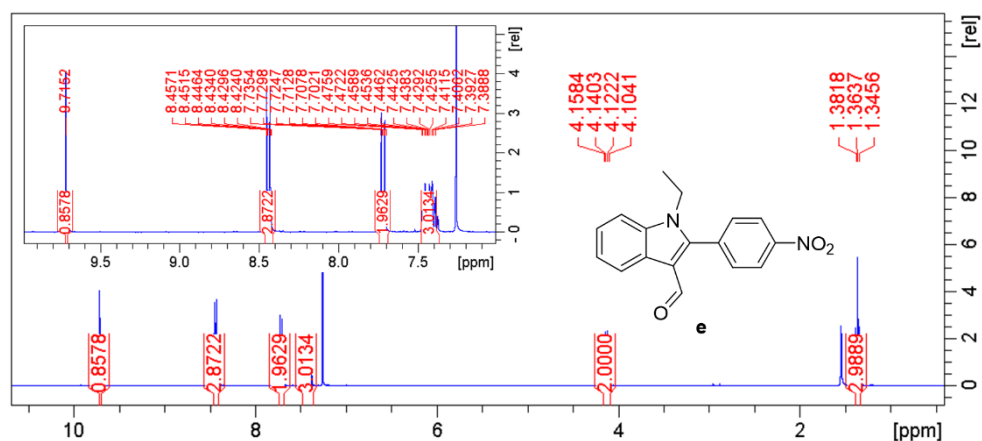


Figure 39. ¹H NMR (400 MHz, CDCl₃) spectrum of **e**.

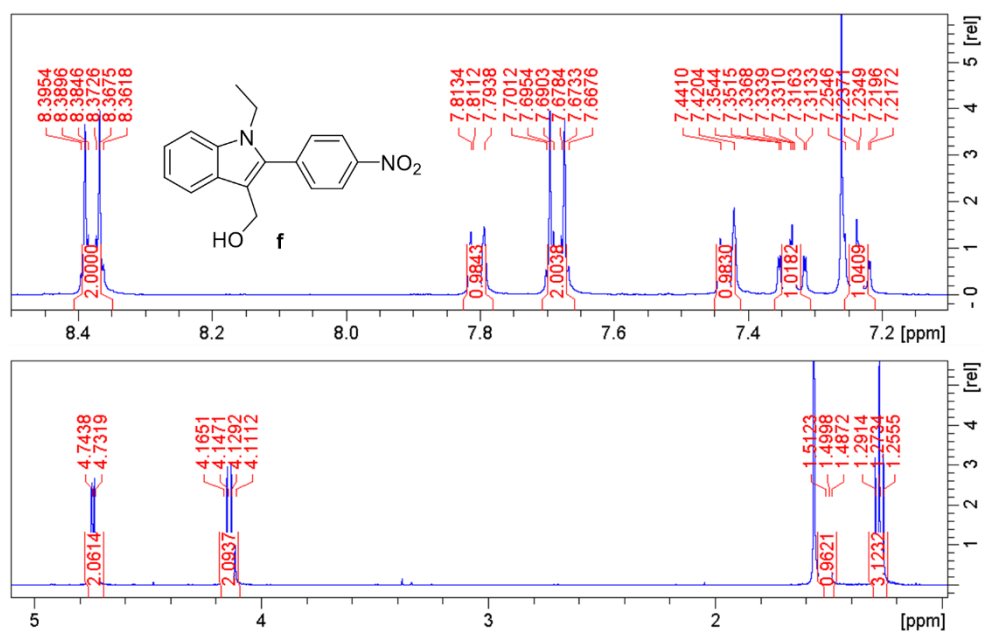


Figure 40. ¹H NMR (400 MHz, CDCl₃) spectrum of **f**.

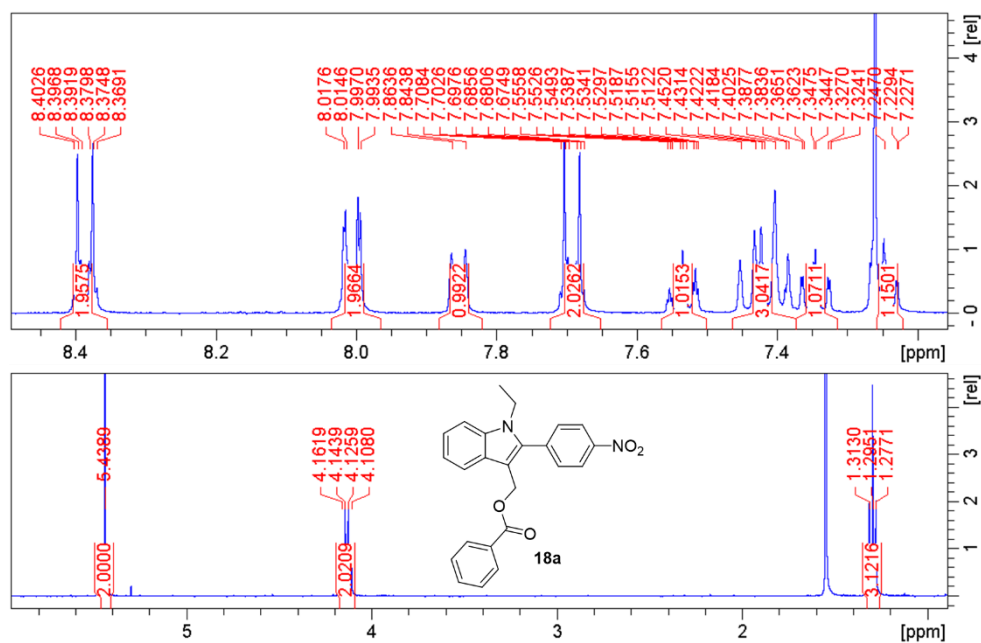


Figure 41. ^1H NMR (400 MHz, CDCl_3) spectrum of **18a**.

Photoreaction of Benzoyl Peroxide in the presence of DMPO.

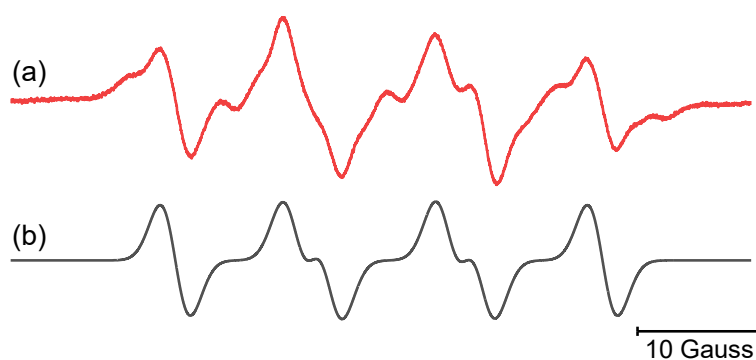
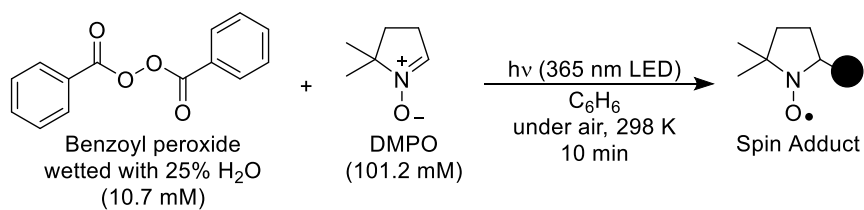
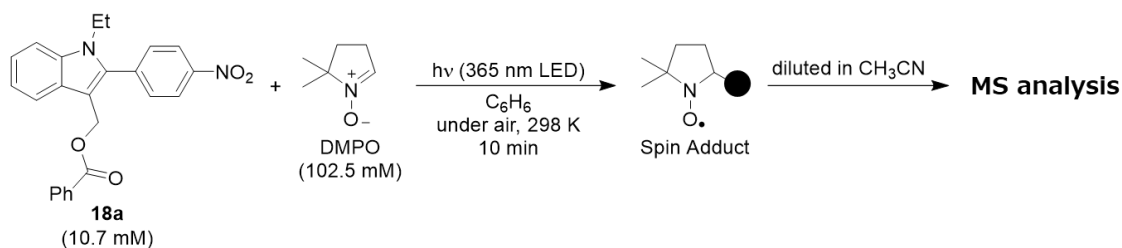
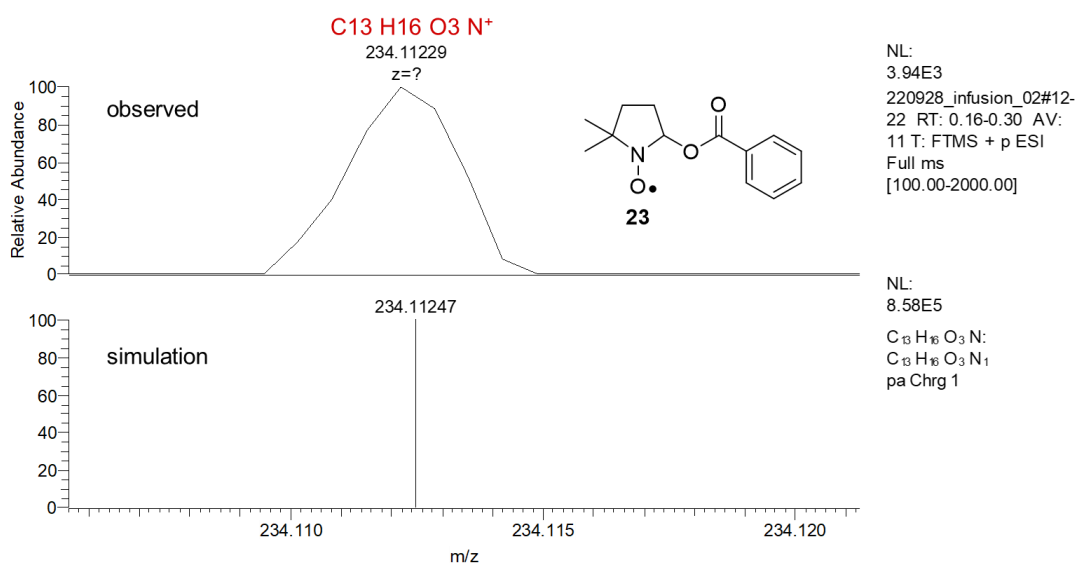


Figure 42. (a) EPR spectrum obtained after the photolysis of benzoyl peroxide with 25% H_2O (10.7 mM) and DMPO (101.2 mM) in benzene using a 365 nm LED lamp. (b) Simulation spectrum of spin adduct DMPO-OC(O)Ph (**23**) ($a_{\text{N}} = 12.37$ G, $a_{\text{H}^\beta} = 9.85$ G).

HRMS (ESI+) spectra of spin adducts generated in the photoreaction of 18a and DMPO. High-resolution mass spectra (HRMS) were performed with a Thermo Fisher Scientific LTQ Orbitrap XL using ionization positive (ESI+; 8 kV, capillary temperature: 100 °C) method.



Scheme 6. Method of detecting spin adducts generated in the photolysis of **18a** (10.7 mM) in the presence of DMPO (102.5 mM) in benzene using a 365 nm LED lamp. The photoreaction solution was diluted in acetonitrile before conducting mass spectrometry measurements.



m/z	Theo. Mass	Delta (ppm)	RDB equiv.	Composition
234.11229	234.11247	-0.77	6.5	$C_{13}H_{16}O_3N$

Figure 43. HRMS (ESI+) observed and simulation spectra of **23**.

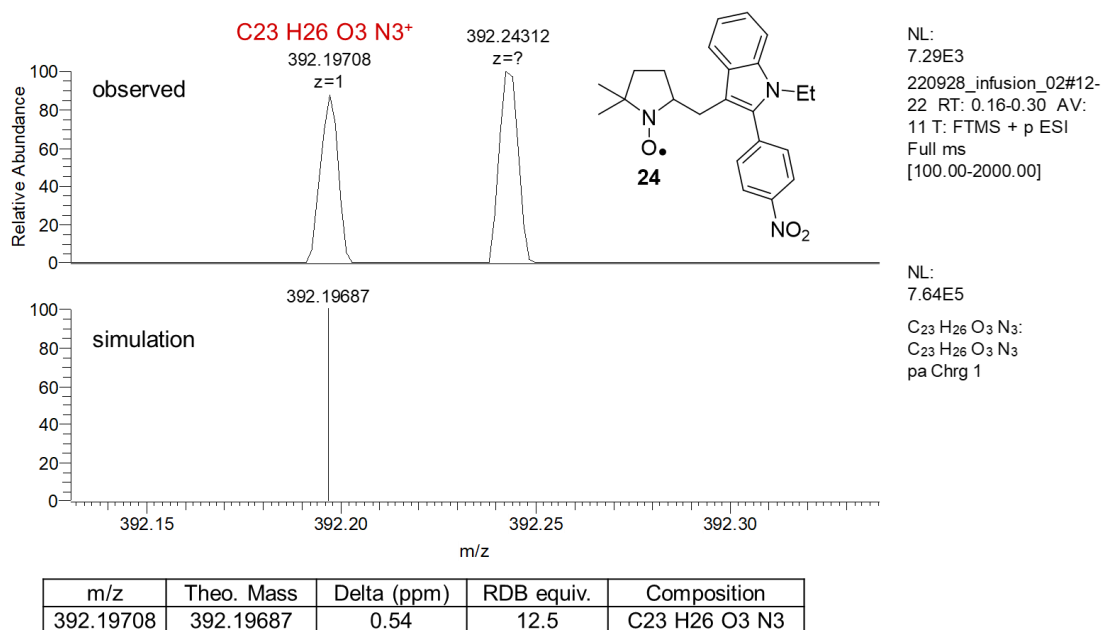


Figure 44. HRMS (ESI+) observed and simulation spectra of **24**.

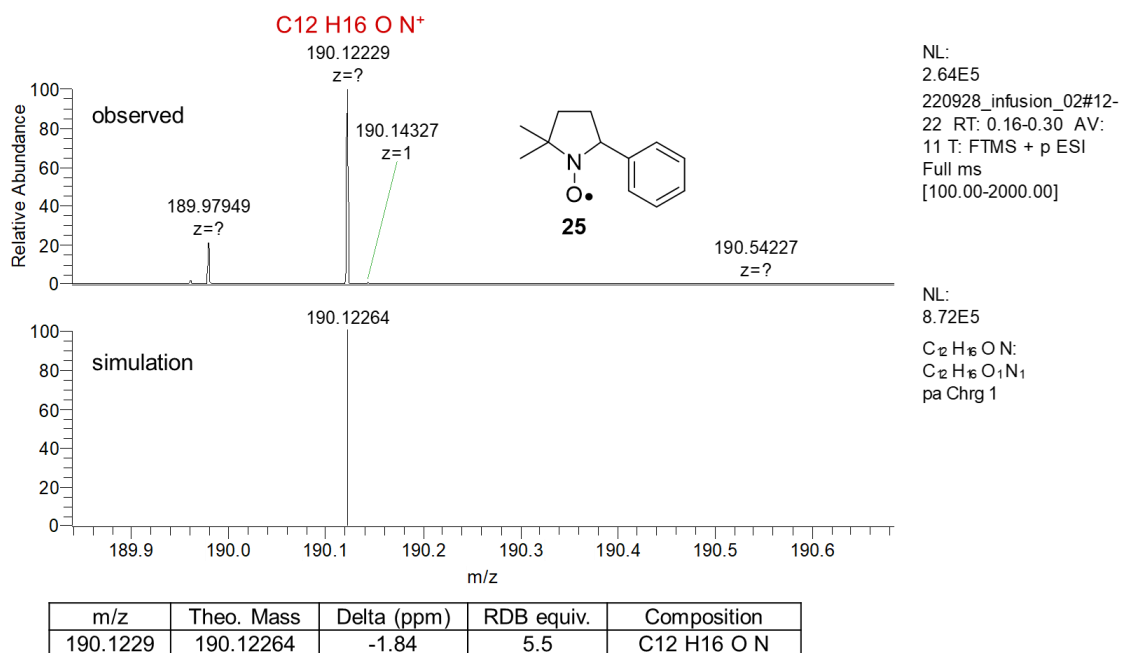


Figure 45. HRMS (ESI+) observed and simulation spectra of **25**.

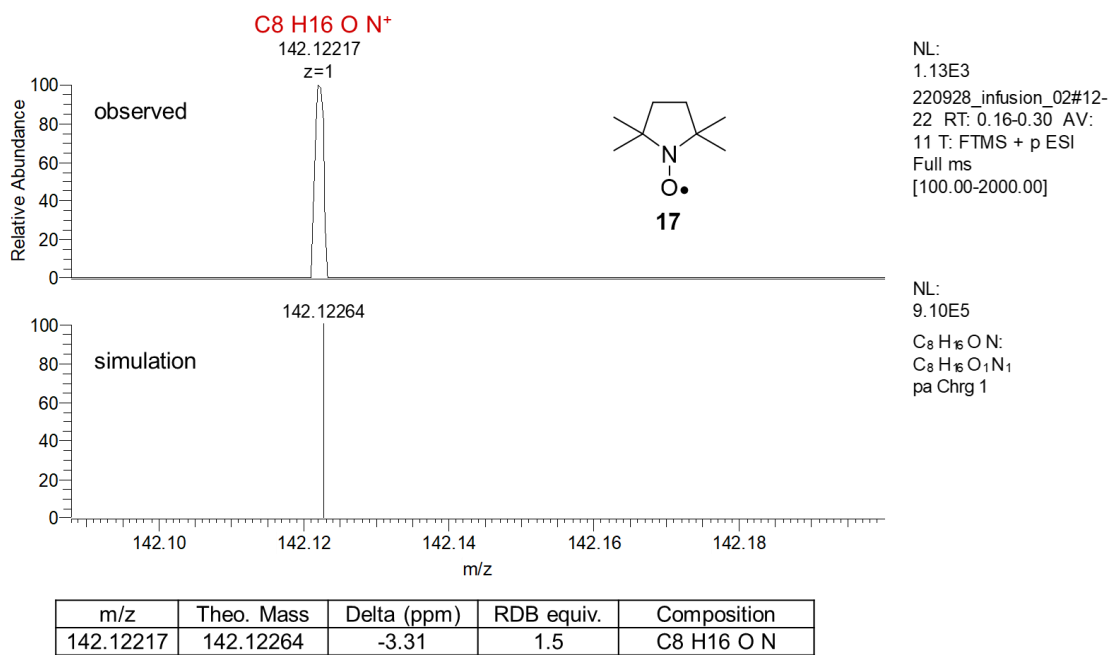


Figure 46. HRMS (ESI+) observed and simulation spectra of **17**.

Chapter 4

Conclusions and Outlook

Conclusions and Outlook:

In this study, the DMPO spin trapping method was used to experimentally observe the radical species generated in organic photoreactions. The radical species generated in the photolysis were identified by observing the spin adducts formed by photoirradiation of a mixture of organic compounds and DMPO using EPR and MS measurements, and by predicting the HFCC values of the spin adducts using quantum chemical calculations. Furthermore, we have succeeded in observing the spin adducts, which have never been reported before, by using this method for the observation of radical species generated by organic photoreactions. This method of analyzing spin adducts can be used to identify radical species generated in various other chemical reactions and is expected to lead to the elucidation of the reaction mechanisms of chemical reactions that have not yet been clarified.

References

- 1 Turro, N. J. *Modern Molecular Photochemistry*, University Science Books, Sausalito, **1991**.
- 2 Lynn, E. V. *J. Am. Chem. Soc.* **1919**, *41*, 368-370.
- 3 Zavoisky, E. K. *Zhur. Eksperiment. i Theoret.* **1945**, *15*, 344-350.
- 4 Janzen, E. G. *Acc. Chem. Res.* **1971**, *4*, 31-40.
- 5 Iwamura, M.; Inamoto, N. *Bull. Chem. Soc. Jap.* **1967**, *40*, 702.
- 6 Iwamura, M.; Inamoto, N. *Bull. Chem. Soc. Jap.* **1970**, *43*, 856-860.
- 7 a) Janzen, E. G.; Liu, J. I. P. *J. Magn. Reson.* **1973**, *9*, 510-512. b) Makino, K.; Hagiwara, T.; Murakami, A. *Int. J. Radiat. Appl. Instrumentation. Part.* **1991**, *37*, 657-665.
- 8 Guo, Q.; Qian, S. Y.; Mason, R. P. *J. Am. Soc. Mass Spectrom.* **2003**, *14*, 862-871.
- 9 Yamaguchi, M. *Comput. Theor. Chem.* **2017**, *1104*, 24-31.
- 10 Gaussian 16, Revision C.01, Frisch, M. J.; Trucks, G. W.; Schlegel, H. B.; Scuseria, G. E.; Robb, M. A.; Cheeseman, J. R.; Scalmani, G.; Barone, V.; Petersson, G. A.; Nakatsuji, H.; Li, X.; Caricato, M.; Marenich, A. V.; Bloino, J.; Janesko, B. G.; Gomperts, R.; Mennucci, B.; Hratchian, H. P.; Ortiz, J. V.; Izmaylov, A. F.; Sonnenberg, J. L.; Williams-Young, D.; Ding, F.; Lipparini, F.; Egidi, F.; Goings, J.; Peng, B.; Petrone, A.; Henderson, T.; Ranasinghe, D.; Zakrzewski, V. G.; Gao, J.; Rega, N.; Zheng, G.; Liang, W.; Hada, M.; Ehara, M.; Toyota, K.; Fukuda, R.; Hasegawa, J.; Ishida, M.; Nakajima, T.; Honda, Y.; Kitao, O.; Nakai, H.; Vreven, T.; Throssell, K.; Montgomery, J. A., Jr.; Peralta, J. E.; Ogliaro, F.; Bearpark, M. J.; Heyd, J. J.; Brothers, E. N.; Kudin, K. N.; Staroverov, V. N.; Keith, T. A.; Kobayashi, R.; Normand, J.; Raghavachari, K.; Rendell, A. P.; Burant, J. C.; Iyengar, S. S.; Tomasi, J.; Cossi, M.; Millam, J. M.; Klene, M.; Adamo, C.; Cammi, R.; Ochterski, J. W.; Martin, R. L.; Morokuma, K.; Farkas, O.; Foresman, J. B.; Fox, D. J. Gaussian, Inc., Wallingford CT, **2016**.
- 11 a) Vydrov, O. A.; Scuseria, G. E. *J. Chem. Phys.* **2006**, *125*, 234109. b) Vydrov, O. A.; Heyd, J.; Krukau, A. V.; Scuseria, G. E. *J. Chem. Phys.* **2006**, *125*, 074106. c) Vydrov, O. A.; Scuseria, G. E.; Perdew, J. P. *J. Chem. Phys.* **2007**, *126*, 154109.
- 12 a) Hehre, W. J.; Ditchfield, R.; Pople, J. A. *J. Chem. Phys.* **1972**, *56*, 2257. b) Hariharan, P. C.; Pople, J. A. *Theor. Chim. Acta* **1973**, *28*, 213-222.
- 13 Marenich, A. V.; Cramer, C. J.; Truhlar, D. G. *J. Phys. Chem. B* **2009**, *113*, 6378-6396.
- 14 Cremer, D.; Pople, J. A. *J. Am. Chem. Soc.* **1975**, *97*, 1358-1367.
- 15 Pickett, H. M. *J. Mol. Spectrosc.* **1991**, *148*, 371-377.
- 16 Yang, B.; Chen, Y.; Shi, J. *Chem. Rev.* **2019**, *119*, 4881-4985.

- 17 Sayin, V. I.; Ibrahim, M. X.; Larsson, E.; Nilsson, J. A.; Lindahl, P.; Bergo, M. *Science Transl. Med.* **2014**, *6*, 221ra15.
- 18 Trachootham, D.; Alexandre, J.; Huang, P. *Nature Rev. Drug. Discov.* **2009**, *8*, 579-591.
- 19 Baciocchi, E.; Bietti, M.; Salamone, M.; Steenken, S. *J. Org. Chem.* **2002**, *67*, 2266-2270.
- 20 a) Paul, H.; Small, R. D., Jr.; Scaiano, J. C. *J. Am. Chem. Soc.* **1978**, *100*, 4520-4527. b) Tsentlovich, Y. P.; Kulik, L. V.; Gritsan, N. P.; Yurkovskaya, A. V. *J. Phys. Chem. A* **1998**, *102*, 7975-7980. c) Weber, M.; Fischer, H. *J. Am. Chem. Soc.* **1999**, *121*, 7381-7388.
- 21 a) Baginée, A.; Howard, J. A.; Scaiano, J. C.; Stewart, L. C. *J. Am. Chem. Soc.* **1983**, *105*, 6120-6123. b) Neville, A. G.; Brown, C. E.; Rayner, D. M.; Luszyk, J.; Ingold, K. U. *J. Am. Chem. Soc.* **1989**, *111*, 9269-9270. c) Avila, D. V.; Brown, C. E.; Ingold, K. U.; Luszyk, J. *J. Am. Chem. Soc.* **1993**, *115*, 466-470. e) Salamone, M.; Bietti, M. *Synlett* **2014**, *25*, 1803-1816. f) Salamone, M.; Bietti, M. *Acc. Chem. Res.* **2015**, *48*, 2895-2903. g) Salamone, M.; Martin, T.; Milan, M.; Costas, M.; Bietti, M. *J. Org. Chem.* **2017**, *82*, 13542-13549. h) Salamone, M.; Ortega, V. B.; Martin, T.; Bietti, M. *J. Org. Chem.* **2018**, *83*, 5539-5545. i) Pipitone, L. M.; Carboni, G.; Sorrentino, D.; Galeotti, M.; Salamone, M.; Bietti, M. *Org. Lett.* **2018**, *20*, 808-811. j) Martin, T.; Salamone, M.; Bietti, M. *Chem. Commun.* **2019**, *55*, 5227-5230.
- 22 Bourgeois, M. J.; Montaudon, E.; Maillard, B. *Tetrahedron* **1993**, *49*, 2477-2484.
- 23 *WinEPR SimFonia*; Weber, R. T. Bruker Instruments, Inc: Billerica, MA, 1995.
- 24 Keana, J. F.; Lee, T. D.; Bernard, E. M. *J. Am. Chem. Soc.* **1976**, *98*, 3052-3053.
- 25 a) Lee, C.; Yang, W.; Parr, R. G. *Phys. Rev. B* **1988**, *37*, 785-789. b) Becke, A. D. *Phys. Rev. A* **1988**, *38*, 3098-3100. c) Miehlisch, B.; Savin, A.; Stoll, H.; Preuss, H. *Chem. Phys. Lett.* **1989**, *157*, 200-206.
- 26 Sandhiya, L.; Zipse, H. *Chem. Eur. J.* **2015**, *21*, 14060-14067.
- 27 Sanhiya, L.; Zipse, H. *J. Comput. Chem.* **2017**, *38*, 2186-2192.
- 28 Luo, Y. -R. *Handbook of Bond Dissociation Energies in Organic Compounds*; VRV Press, 2002.
- 29 Hendrickson, W. H.; Nguyen, C. C.; Nguyen, J. T.; Simons, K. T. *Tetrahedron Lett.* **1995**, *36*, 7217-7220.
- 30 Matsumoto, S.; Naito, M.; Oseki, T.; Akazome, M.; Otani, Y. *Tetrahedron*, **2017**, *73*, 7254-7259.
- 31 Klán, P.; Šolomek, T.; Bochet, C. G.; Blanc, A.; Givens, R.; Rubina, M.; Popik, V.;

- Kostikov, A.; Wirz, J. *Chem. Rev.* **2013**, *113*, 119-191.
- 32 Lin, Q.; Guo, R.; Hamao, K.; Takagi, R.; Abe, M. *Chem. Lett.* **2022**, *51*, 153-156.
- 33 Yoshimi, Y.; Itou, T.; Hatanaka, M. *Chem. Commun.* **2007**, 5244-5246.
- 34 Ishiyama, T.; Takagi, J.; Nobuta, Y.; Miyaura, N. *Org. Synth.* **2005**, *82*, 126-133.
- 35 Xu, X. H.; Liu, G. K.; Azuma, A.; Tokunaga, E.; Shibata, N. *Org. Lett.* **2011**, *13*, 4854-4857.
- 36 Roagna, G.; Ascough, D. M. H.; Ibba, F.; Vicini, A. C.; Fontana, A.; Christensen, K. E.; Peschiulli, A.; Oehlrich, D.; Misale, A.; Trabanco, A. A.; Paton, R. S.; Pupo, G.; Gouverneur, V. *J. Am. Chem. Soc.* **2020**, *142*, 14045-14051.

List of Publications

公表論文

(1) “Reactivity and Product Analysis of a Pair of Cumyloxy and *tert*-Butoxyl Radicals Generated in Photolysis of *tert*-Butyl Cumyl Peroxide”

Ryoko Oyama and Manabu Abe*

J. Org. Chem. **2020**, *85*, 8627-8638.

(2) “DMPO Spin Trapping Study of the Photolysis of 2-(4-Nitrophenyl)-1*H*-indolyl-3-methyl Derivatives”

Ryoko Oyama, Ryuei Hayashi, and Manabu Abe*

Chem. Lett. **2023**, *52*, 10-12.

参考論文

(1) “Design and Synthesis of Two-Photon Responsive Chromophores for Near-Infrared Light-Induced Uncaging Reactions”

Manabu Abe,* Youhei Chitose, Satish Jakkampudi, Pham Thi Thu Thuy, Qianghua Lin, Bui Thi Van, Ayato Yamada, Ryoko Oyama, Miyu Sasaki, and Claudine Katan*

Synthesis, **2017**, *49*, 3337–3346.

(2) “Simple generation of various α -monofluoroalkyl radicals by organic photoredox catalysis: modular synthesis of β -monofluoroketones”

Ryo Taniguchi, Naoki Noto, Seiya Tanaka, Keigo Takahashi, Sujan K.

Sarkar, Ryoko Oyama, Manabu Abe, Takashi Koike,* and Munetaka Akita*

Chem. Commun. **2021**, *57*, 2609-2612.

Acknowledgment

All the research works described in this dissertation have been carried out under the guidance of Professor Manabu Abe at the Department of Chemistry, Graduate School of Advanced Science and Engineering, Hiroshima University. My research work was supported by JST SPRING (JPMJSP2131).

First and foremost, I am extremely grateful to my supervisor, Professor Manabu Abe for his invaluable advice, continuous support, and patience during my Ph.D. study. I would also like to thank Lecturer Sayaka Hatano and Assistant Professor Ryukichi Takagi for their technical support and discussion on my study. I would like to thank all the members of our laboratory. It is their kind help and support that have made my research study and life in an excellent time. I also thank N-BARD, Hiroshima University, for providing the EPR measurement facilities and for assistance with the MS measurements.

Finally, I would like to express my gratitude to my family, especially my parents for their kindness and support, and for giving me birth. I would also like to thank my lovely Java sparrows for all the entertainment and emotional support.



Ryoko OYAMA

Research group of Reaction Organic Chemistry,
Department of Chemistry,
Graduate School of Advanced Science and Engineering,
Hiroshima University
February 2023